Journal of Power Sources 304 (2016) 207–233

Contents lists available at ScienceDirect

Journal of Power Sources

journal homepage: www.elsevier.com/locate/jpowsour

Review article

# Performance and degradation of Proton Exchange Membrane Fuel Cells: State of the art in modeling from atomistic to system scale

T. Jahnke [a,*], G. Futter [a], A. Latz [a], T. Malkow [b], G. Papakonstantinou [b], G. Tsotridis [b], P. Schott [c,d], M. Gérard [c,d], M. Quinaud [c,d], M. Quiroga [e,f], A.A. Franco [e,f,g], K. Malek [h,i], F. Calle-Vallejo [j], R. Ferreira de Morais [j], T. Kerber [j], P. Sautet [j], D. Loffreda [j], S. Strahl [k], M. Serra [k], P. Polverino [l], C. Pianese [l], M. Mayur [m], W.G. Bessler [m], C. Kompis [n]

[a] German Aerospace Center (DLR), Institute of Engineering Thermodynamics, Pfaffenwaldring 38-40, 70569 Stuttgart, Germany
[b] European Commission, Directorate-General Joint Research Centre (JRC), Institute for Energy and Transport (IET), Postbus 2, 1755 ZG Petten, The Netherlands
[c] Univ. Grenoble Alpes, F-38000 Grenoble, France
[d] CEA LITEN, DEHT, F-38054 Grenoble, France
[e] Laboratoire de Réactivité et Chimie des Solides (LRCS) – Université de Picardie Jules Verne & CNRS, UMR 7314 – 33 rue Saint Leu, 80039 Amiens, France
[f] Réseau sur le Stockage Electrochimique de l'Energie (RS2E), FR CNRS 3459, France
[g] ALISTORE-ERI European Research Institute, FR CNRS 3104, 80039 Amiens Cedex, France
[h] Department of Chemistry, Simon Fraser University, 8888 University Dr, Burnaby BC V5A 1S6, Canada
[i] NRC-EME, 4250 Wesbrook Mall, Vancouver BC V6T 1W5, Canada
[j] Université de Lyon, Ecole Normale Supérieure de Lyon, CNRS, Laboratoire de Chimie, 46 Allée d'Italie, F-69364 Lyon Cedex 07, France
[k] Institut de Robòtica i Informàtica Industrial (CSIC-UPC), Parc Tecnològic de Barcelona, C/Llorens i Artigas 4-6, 08028 Barcelona, Spain
[l] Department of Industrial Engineering, University of Salerno (UNISA), Via Giovanni Paolo II, 132, Fisciano, SA, Italy
[m] Institute of Energy Systems Technology (INES), Offenburg University of Applied Sciences, Badstrasse 24, 77654 Offenburg, Germany
[n] Vodera Ltd., 145-157 St John St, EC1V 4PY London, United Kingdom

## HIGHLIGHTS

- We review PEMFC models ranging from the atomistic scale up to the system level.
- We review multiscale approaches for the coupling between the scales.
- We review degradation models for all PEMFC components.
- Advantages, drawbacks and open issues of the models are discussed.

## ARTICLE INFO

*Article history:*
Received 9 May 2015
Received in revised form 14 October 2015
Accepted 9 November 2015
Available online 6 December 2015

*Keywords:*
Proton Exchange Membrane Fuel Cells
Modeling
Performance
Degradation

## ABSTRACT

Proton Exchange Membrane Fuel Cells (PEMFC) are energy efficient and environmentally friendly alternatives to conventional energy conversion systems in many yet emerging applications. In order to enable prediction of their performance and durability, it is crucial to gain a deeper understanding of the relevant operation phenomena, e.g., electrochemistry, transport phenomena, thermodynamics as well as the mechanisms leading to the degradation of cell components. Achieving the goal of providing predictive tools to model PEMFC performance, durability and degradation is a challenging task requiring the development of detailed and realistic models reaching from the atomic/molecular scale over the meso scale of structures and materials up to components, stack and system level. In addition an appropriate way of coupling the different scales is required.

This review provides a comprehensive overview of the state of the art in modeling of PEMFC, covering all relevant scales from atomistic up to system level as well as the coupling between these scales. Furthermore, it focuses on the modeling of PEMFC degradation mechanisms and on the coupling between performance and degradation models.



* Corresponding author.
*E-mail address:* thomas.jahnke@dlr.de (T. Jahnke).

http://dx.doi.org/10.1016/j.jpowsour.2015.11.041
0378-7753/

## 1. Introduction

Polymer Electrolyte Membrane Fuel Cells (PEMFCs) represent one of the most promising systems for both stationary and automotive applications (e.g. power generation and on-board application for hybrid vehicles). However, focusing on these latter ones, PEMFCs still present critical issues concerning system technology, design, fuel storage, system control and durability. To ensure the optimal operation, the fuel cell (FC) stack requires several auxiliary components (i.e. Balance of Plant – BoP), such as blowers, humidifiers, water pumps, etc. Although the correct design of the stack is a core issue, the whole system efficiency depends on the behavior of both the stack and the BoP, which also require an optimized design. To enhance the development and the control of a PEMFC system, mathematical models can be of help by contributing to the reduction of development time and costs by means of system prototyping and testing. Furthermore, models can also be exploited for diagnostic purposes, to identify the main unhealthy behaviors and their causes in order to define and improve suited control strategies. For this reason, a comprehensive PEMFC system model is required. In the literature, many models have been developed to describe PEMFCs physical behaviors [1–5], but some of them focus only on specific phenomena without considering the complex interaction among the components. An example closely related to PEMFC system is the identification of the optimal water content to ensure the highest efficiency at different operating conditions. Indeed, membrane hydration must be maintained within specific limits to ensure correct functioning (i.e. high proton conductivity). An excess of water (i.e. flooding) leads to a decline in cell performance due to clogging in the porous layers and channels of the cell, while membrane dry-out results in it being degraded and, consequently, to system failure [6]. Furthermore, most of the available models are not genuinely predictive due to their lack of accurate description of specific phenomena, like liquid water formation and transport [7].

In addition to accurately describe all relevant physico-chemical mechanisms themselves, a main challenge in modeling of PEMFC is the interplay of these mechanisms occurring on a wide range of time and length scales (Fig. 1). Depending on the scale, specific modeling approaches and experimental validation methods are applicable. In order to obtain a really predictive model, all relevant scales have to be taken into account and the models on all scales have to be coupled appropriately.

In this review we focus on this multiscale aspect, describing the different modeling approaches on all relevant scales as well as the coupling between these models.

In the first part (Section 2) we present the state of the art in modeling of PEMFC performance at the different scales. After reviewing first-principle approaches at the atomic level (Sec. 2.1) and microscale simulations (Sec. 2.2), we turn to the modeling on cell level (Sec. 2.3). After an overview over single-cell models (Sec. 2.3.1), we discuss the models developed for the different cell components, i.e., for the membrane (Sec. 2.3.2), the electrodes (Sec. 2.3.3), the GDLs (gas diffusion layers) (Sec. 2.3.4) and the interface between GDL and gas flow channel (Sec. 2.3.5). Subsequent to the cell level we review the modeling done on stack and system level (Sec. 2.4). The first part is completed with a section on the coupling between the scales, i.e., multiscale model approaches (Sec. 2.5).

The second part (Section 3) of this review is dedicated to the modeling of degradation mechanisms in the different components of a PEMFC. After discussing the thermal, mechanical and chemical degradation of the membrane (Sec. 3.1), we turn to the degradation mechanisms of the catalyst layer (Sec. 3.2), the GDL (Sec. 3.3) and the bipolar plates (Sec. 3.4). We conclude this part with a section on the coupling between performance and degradation models (Sec. 3.5), which is of particular importance in order to obtain a model with lifetime predictive capabilities.

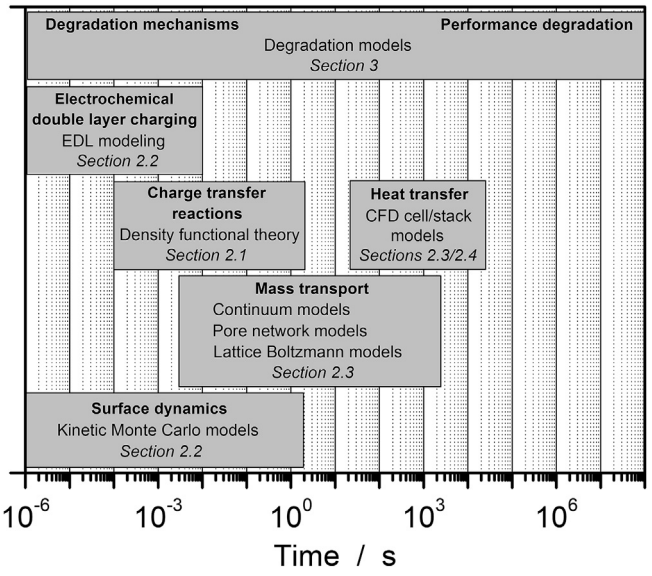


**Fig. 1.** Schematic of time scales of key processes taking place inside PEMFC including respective modeling approaches to describe these processes or provide information about them. Time scales for the processes are based on Ref. [359]. Note that the modeling methods do not necessarily cover the same time scales, e.g., DFT provides important insight on the reaction kinetics even though the time scale considered in such ab initio techniques is very small (ranging from femtoseconds to about one nanosecond). Also note that the physiochemical degradation processes occur on short time scales, while their effect on cell performance becomes noticeable only at much larger timescales. This gives rise to the development of mechanistic degradation models at short time scales and lifetime prediction models covering the large timescales.

## 2. Modeling of PEMFC performance

### 2.1. First-principle approaches at the atomic level

The Oxygen Reduction Reaction (ORR) is among the current fundamental challenges in the domains of energy and environment, as it is one of the main bottlenecks for the PEMFC design and application [8,9]. The large-scale commercialization of PEMFC for the demanding applications of the automotive industry is currently hindered by the kinetic limitations of the ORR [10–12]. The restrictions imposed by the ORR are related to the substantial overpotential at practical current densities, to the required decrease of platinum loading needed to reduce the cost for automotive applications as well as the prevention of Pt dissolution [11]. The reaction occurs on carbon supported platinum particles [13,14]. Although a significant number of experimental and theoretical works have been proposed in the literature to understand this reaction on model surfaces of Pt and its alloys [15–17], important questions related to the effects of support, solvent (water, pH), and particle size and morphology in the catalytic activity and stability remain far from being elucidated.

Regarding the electrocatalytic tests in model conditions, various authors have proposed different syntheses such as reduction of platinum-based organometallic complexes [13], single-atom-to-cluster method [14], dendrimer or colloidal methods [18] and cathodic corrosion [19], among others, in order to control the size of Pt-based nanocatalysts and to measure the intrinsic catalytic activity towards ORR and Hydrogen Oxidation Reaction (HOR). According to recent experimental studies, there is a strong controversy regarding the optimal size of the particles for the

electrocatalytic activity of both HOR and ORR. In the range of 2.5–28 nm, some authors claim that the catalytic activity for HOR or ORR activity increases with decreasing particle size [20,21], whereas others did not observe any change for ORR in the range of 5–10 nm [22]. More recently, a high ORR activity has been observed for certain sizes (1.8 and 3.4 nm) [13]. Besides, it is striking that Pt sub-nanometer particles, e.g., $Pt_{12}$ clusters, can have electrocatalytic activities that are one order of magnitude larger than those of reference Pt/C catalysts [18].

Moreover, the most active site of the nanoparticle catalyst (apex, edge, larger (100) or (111) facets) has not been clearly identified yet. Recently, some authors have suggested surface steps to play a minor role in the overall ORR activity [14], whereas some others have indicated the high activity of terrace atoms near step edges in Pt single crystals [23].

The electrochemical environment in which the ORR takes place is rather complex and its theoretical modeling and simulation requires numerous assumptions and simplifications [24]. One of the most widespread models is based on the so-called computational hydrogen electrode which uses Density Functional Theory (DFT) calculations of gas-phase systems to describe electrochemical systems. The link between those two different environments is made through the thermodynamic equilibrium between $\frac{1}{2}H_2(g)$ and $(H^+ + e^-)$ [15,24]. This equilibrium allows for the inclusion of both pH and applied potential effects in the models, making it possible to predict onset potentials, overpotentials and surface Pourbaix diagrams [15,24,25]. However, the model is limited to coupled proton-electron transfers and does not include explicit solvent molecules, so that solvation corrections must be added manually [24,26]. Recently, more general models have emerged that revisit pH effects and proton-electron transfer in more general ways [27–29].

It is noteworthy that most of the studies in the literature are devoted to extended surfaces. There are only a few theoretical studies that tackle the problem of the interaction between platinum particles and the reaction intermediates involved in the ORR mechanism. Those models are based on Pt clusters (from a few atoms [30,31] up to hundreds [32–36]) either in vacuum or using polarizable continuum model (PCM) calculations to implicitly account for solvent effects [37]. So far, various theoretical studies have shown the competition between two key elementary steps in the mechanism: the dissociation of $O_2$ either through a direct route (producing two *O species)[1] or through the formation of *OOH and the subsequent formation of *OH surface species [15,24,31,38–40]. However, the mechanism has not yet been explored directly on a nano-size particle model, neither in vacuum nor in a solvent, although recent studies have started to address particle-size effects on the ORR activity of Pt nanoparticles [41,42]. It is important to note that size effects have traditionally hindered the direct comparison between nanoparticles and extended surfaces. Recently, the adsorption energies of various ORR intermediates have been studied on Pt nanoparticles of various sizes and extended surfaces [34]. It was found that the corresponding trends are captured linearly by using "generalized coordination numbers". By the use of this generalized descriptor, new activity–structure relations were proposed very recently to sort the catalytic properties of various Pt nanoparticles and extended surfaces [36]. By combining DFT calculations and electrochemical measurements, it was shown that new pure Pt catalytic surfaces presenting regular hexagonal cavities offer a significantly improved electrocatalytic performance regarding ORR, with respect to Pt(111) and other Pt-based alloys. To date, some attempts exist to provide explicit descriptions of the water/platinum extended liquid/metal interface [29,43], but there are no reports on explicitly solvated platinum nanoparticles. These highly challenging systems have not been considered so far, as their modeling requires large computational resources.

Model experiments on single-crystal surfaces have also been proposed to investigate the elementary mechanism of the catalytic formation of water on Pt(111) under ultrahigh vacuum (UHV) by scanning tunneling microscopy (STM), high resolution electron energy loss spectroscopy (HREELS), low energy electron diffraction (LEED) and temperature programmed desorption (TPD) [44,45]. It has been shown that below the desorption temperature (180 K under ultra high vacuum conditions), water can react with adsorbed unreacted atomic oxygen to form hydroxyl surface species, hence leading to an autocatalytic process, whereas at higher temperatures the sequential addition of adsorbed atomic hydrogen and oxygen takes place with normal kinetics. In addition, no peroxide species has been detected. Nonetheless, other investigations with molecular beam relaxation spectroscopy in the temperature range of 300–1200 K or in-situ mass spectrometry and post-reaction TPD at 85 K suggest alternatively the existence of a fast $H_2O_2$ surface species or an *OOH intermediate [46,47].

During the last decade, numerous theoretical works have been proposed to tackle these controversial interpretations regarding the elementary steps [9,26,48–51]. Firstly, several groups have elucidated simple elementary steps at the level of gas/Pt(111) models in periodic boundary conditions (PBC), starting from molecular oxygen dissociation [52–55], water formation through an *O + *H pathway [56] and then, disproportionation routes [38,57] and water formation through an *OOH pathway [58]. Secondly, more systematic studies have been proposed to combine these competitive elementary steps and to conclude about the preferential elementary mechanism [39,48,59]. During the past few years, significant efforts have been devoted to probe the influence of the aqueous solution on the ORR mechanism [37,60–67], either by considering continuum models [37] or by treating explicitly a small number of water molecules [60,62,65–67] such as ice bilayers [61,63], or confined static water [64]. At the same time, the influence of the applied electric field has been evoked in the literature [15,26,48,68–72] either by thermodynamic approaches such as the computational hydrogen electrode [15,24,26,48,69,70,72–75], by first-principles based mean-field or multiscale models [50,51,76,77] or by self-consistently minimized DFT schemes [68,71].

Interestingly, the majority of the DFT studies in PBC at the classical gas/Pt(111) model describe the reaction mechanism of water formation and ORR at medium or high surface coverage (>1/4 ML, mono layers) [38,48,59]. One of the key questions is related to the elementary mechanism of the O–O bond breaking from $O_2$ and the subsequent formation of the *OH species. A close comparison of the two most likely scenarios, i.e., direct dissociation or OOH-mediated path, indicates that the direct route is less favorable due to a series of high activation barriers for molecular dissociation (0.71 eV) and *OH formation via *O + *H (0.72 eV) [48]. In contrast, the OOH-mediated route offers a sequence of low activation energies for $O_2$ + H association (0.29 eV) and *O + *OH dissociation (0.16 eV). Finally, for this coverage, the formation of hydrogen peroxide from *OOH species is predicted to be disfavored due to a slightly larger barrier (0.21 eV) compared to its quasi-spontaneous dissociation into *O + *OH (0.16 eV) [48]. Recently, the influence of *OH surface coverage on the competition between $^*O_2$ dissociation and *OOH formation has been investigated on Pt(111) [39]. For *OH coverage below 0.3 ML, the direct dissociation is preferential, whereas *OOH formation becomes favored for coverage above 0.3 ML. As soon as atomic oxygen is formed and water is present on the catalyst surface (either produced by the reaction or coming from the solution), the disproportionation reactions between $2H_2O$ and 1O may occur at higher surface coverage (~3/4 ML) and can open a less

[1] Superscript * denotes surface species.

activated alternative mechanism for the formation of *OH surface species (0.12 eV) [38]. Increasing the potential at room temperature significantly changes this picture, generally by an increase of the activation barriers (loss of catalytic activity) and by poisoning the catalyst with more stable adsorbed *O and *OH species [48,70]. However, these remarkable observations are contradicted by other authors [69], who have observed little or no influence of applied electric fields on adsorption energies.

Taking into account the aforementioned findings, we conclude that computational electrochemistry is a field still in development that has provided significant insight into the ORR mechanism on Pt, but that the answers to several important questions are still elusive. In spite of contradicting observations, the field is slowly reaching consensus about the reaction intermediates and their relative importance and correlations between adsorption energies [78,79], while the number of effects included in the calculations keeps increasing. As mentioned before, recent works have started to theoretically address the influence of the nanoparticle size and the geometric environment around the active sites on the adsorption energies and the ORR activity [34,41], but this kind of studies is not widespread yet, due to the large computational resources required. Solvation, sintering and degradation effects remain open issues and there are no studies that consider all these possible effects coupled to the electrocatalytic behavior within a single simulation [80]. Instead, the literature is composed of collections of deconvolved effects that lack a sense of generality. Thus, the major challenges in the computational modeling of the ORR are currently the inclusion of the largest possible number of effects and the improvement of their descriptive and predictive power, so that the theoretical representation of the electrode-support-electrolyte interface is as realistic as possible [24]. This is what is summarized in Fig. 2, where the current theoretical approach for the design of ORR electrocatalysts is sketched. Essentially, a given surface property, namely an electronic [81], geometric [34] or thermodynamic parameter [78,81], often called descriptor, is used to describe the trends in adsorption energies and/or catalytic activities. The latter can either be theoretically estimated as the free energy of reaction of the potential-determining steps or experimentally measured current densities.

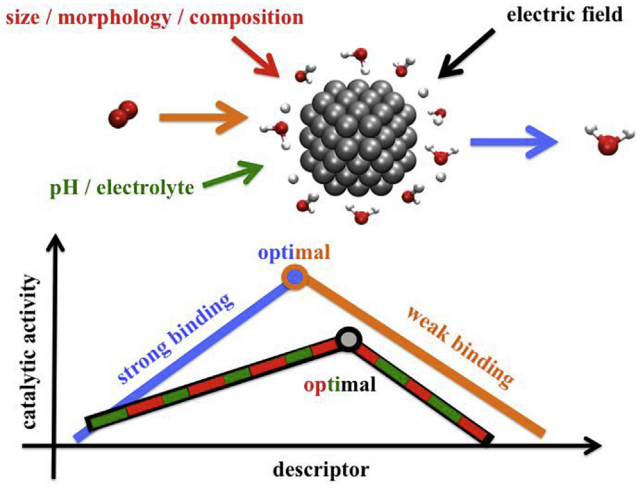


**Fig. 2.** Schematics of Sabatier-type volcano plots. The blue and orange lines represent the usual approach based only on the adsorption strength of the adsorbates to the catalyst surface. The black-green-red lines represent the real situation in which several other effects (catalyst composition and morphology, environment) are taken into account in addition to binding in order to provide realistic predictions. (For interpretation of the references to color in this figure legend, the reader is referred to the web version of this article.)

Ideally, when a wide range of materials is covered, a volcano-type curve should appear in which the activity initially grows up to a maximum, after which it decays. Thus, optimal catalysts exhibit a compromise in the adsorption strength of reactants and products (blue and orange lines), in line with the Sabatier principle. More sophisticated and consequently more accurate volcano plots should include the effects of pH and electrolyte, applied electric field and catalysts' size, morphology and composition, in order to confirm the predictions of simplified approaches or make different, more accurate predictions.

### 2.2. Microscale simulations

In the frame of the multiscale modeling, the so-called electrochemical double layer (EDL) plays an important role in the redox kinetic processes [82–85]. Classical models which describe EDL in equilibrium conditions have been extended to treat non equilibrium conditions representative of PEMFC environments [83]. The extensions proposed assume the EDL to be formed by two regions, the Diffuse Layer and the Compact Layer. The Diffuse Layer model describes the proton transport, affected by the water and/or the morphology of the charged polymer (e.g. Nafion®) at the vicinity of the catalyst surface. The Compact Layer model describes the coverage evolution of the intermediate reaction species (involved in the REDOX reactions) as well as adsorbing/desorbing water molecules on the substrate surface.

Significant efforts have been made in scaling up the EDL modeling from atomistic and molecular level properties to overall performance cell models [51,77,83,86,87]. Proton transport in the EDL is usually modeled within the Poisson–Nernst–Planck framework, not considering electrostatic screening of water in the effective proton transport properties. Recently, a more complete multiscale model describing in detail the interplay between the EDL structure and DFT-based elementary kinetics has been developed [84,88] where the detailed influence of the Nafion® structure and the finite size and polarization effects of both water and solvated protons were considered to calculate the electrode potential as function of the imposed current density.

The Kinetic Monte Carlo (kMC) method plays an important role in the description of surface dynamics, coverage evolution, adsorption, desorption and reaction rates involved in chemical surface, specially for those systems where the Mean Field theory cannot be applied, that is, when the catalyst surface is not homogeneous (e.g. presence of defects) and/or adspecies diffusion and lateral interaction between adspecies play an important role, also when metal surface degradation takes place. In principle kMC is an algorithm that computes random hops from one surface state to another. The complexity of the chemical events that takes place on the surface makes the study under first-principle electronic structure calculations unfeasible. Otherwise, first-principle theories, like DFT, are able to study isolated events and provide kinetic parameters to be implemented in kMC. This methodology is well described by Reuter [89]. In a few words, kMC treats the molecular events as a simple Markov walk, hence, the evolution in time of the probability density function $P_i$ to find the system in state $i$ is described by a master equation of Markovian form [90].

$$\frac{dP_i(t)}{dt} = -\sum_{j\neq i} k_{ij} P_i(t) + \sum_{j\neq i} k_{ji} P_j(t) \quad (1)$$

where $k_{ij}$ is the average escape rate from basin $i$ to basin $j$. This rate can be obtained, for example, from Transition State Theory (TST) taking the activation barriers from DFT calculations. kMC postulates that during thermal vibrational motion the system loses memory, which means that the system has the same probability of

finding the escape path from $i$ to $j$ ($P_{ij}$) during each short time increment $\Delta t$, leading to an exponential decay statistics [89]. This is expressed in the Poisson distribution:

$$P_{ij}(t) = k_{ij} \exp(-k_{ij}\Delta t). \quad (2)$$

This suggests an algorithm, called First-Reaction Method [91], that consists of creating a list of possible rates, generating a time occurrence for each reaction $\Delta t_{ij} = -ln(\rho_i)/k_{ij}$ (where $\rho_i$ is a random number between 0 and 1); executing the event with smallest $\Delta t_{ij}$; update time $t + \Delta t_{ij}$ and recalculating all rates.

One common expression for the kinetic rate is the Arrhenius form

$$k_{ij} = f_{ij} \exp(-E_{ij}/k_B T) \quad (3)$$

where $f_{ij}$ is a pre-exponential factor depending on the vibrational frequency of the transition state, $E_{ij}$ is the activation barrier between the two states $i$ and $j$ while $k_B$ and $T$ are the Boltzmann constant and the absolute temperature, respectively.

Another common kMC algorithm used is the Variable Step Size Method (VSSM) [92]. This algorithm is really fruitful to study those systems where different time scales are involved [93,94]. However, the VSSM may demand a high computational cost, since the algorithm needs to compute all the possible events to execute the event for each kMC step. To reduce the computational cost or to lead to the computational parallelizable scheme, other methods like the First Reaction Method (FRM) and Random Selection Method (RSM) have been developed. FRM consists in an evaluation of those event that may be executed soonest and then execute it, although this method fails in the description of those systems when many different time scales are involved. RSM is based on the hypothesis that the system is homogenous and on a random selection of the reaction will take place. This algorithm is suitable for computational parallelization, however, the method does not allow to study inhomegenities such as surface clustering or located inactive sites. All these methods are well described and compared elsewhere [95].

In the context of PEMFCs, Zhdanov [96] utilized MC simulation to study the kinetics of oxygen electrochemical reduction on Pt and found that this reaction may be nearly first order in oxygen under a wide range of reaction conditions even if the O coverage is appreciable and the O mobility is low. Zhdanov proposed that the reactant coverage is not first order in the $O_2$ reaction. Abramova et al. [97] studied the $O_2$ adsorption on fcc(111) metals by kMC. By taken into account seven elementary steps, they report the total oxygen coverage profile in terms of $\sigma$ (charge density) and sticking probability reporting a strong coverage dependency in the pre-exponential factor.

In 2008, Rai et al. [98] reported the electrochemical discharge of water on Pt(111) by kMC VSSMb supported with first-principle Local Reaction Center (LRC) theory. One of the remarkable results is that OH is the dominant adsorbate between 0.5 and 0.8 V electrode potential, but above 0.8 V, $OH_{ads}$ and $O_{ads}$ coexist. In that work, the OH adsorbed reported a $\sqrt{3} \times \sqrt{3}$ structure and partially ordered structure of O adsorbates results in lean $O_{ads}$ coverage of 0.11 at around 0.9 V in agreement with experimental data [99].

Very recently, a KMC model has been reported which extends the VSSM to electrochemical conditions [100]. This constitutes the first VSSM extension reported so far which allows calculating the electrode potential as function of the imposed current density. The KMC model describes the electrochemical kinetics and it is coupled on the fly with continuum modeling modules describing reactants transport at the active material/electrolyte nanoscopic interface (electrochemical double layer region) and along the mesoscale electrode thickness.

*2.2.1. Self-organization phenomena in PEMFCs*

Despite recent progress in developing multiscale modeling approaches [101] enormous challenges remain in bridging atomistic simulations of realistic structures and continuum models that describe the operation of functional materials for PEMFC applications. While full multiscale methods will not be available in the near future, mesoscale molecular simulation techniques can close the gap between atomistic simulations and macroscopic properties of the system. Such simulations provide vital insight into aspects that have to be considered in fabrication and operation of advanced materials for PEMFC.

To improve structure–performance relationships of PEMFC components, particularly those of catalyst layers (CLs), preparation methods exploit variations in terms of applicable solvent, particle sizes of primary solid powders, wetting properties of support materials, and composition of the catalyst layer ink [102–104]. These factors determine the complex interactions between Pt/carbon particles, ionomer molecules and solvent molecules and, therefore, control the catalyst layer formation process. Mixing the ionomer with dispersed Pt/C catalysts in the ink suspension prior to deposition will increase interfacial surface area between the ionomers and Pt/C nanoparticles. The kind of dispersion medium determines whether ionomer is to be found in solubilized, colloidal or precipitated form. This influences the microstructure and pore size distribution of the CL [105,106]. In general, catalytic activity depends on the electrode composition and structure with well-attuned pore size distributions and wetting properties of the pore network.

Molecular-based simulations at mesoscale level provide insights into segregation, structural correlations and dynamical behavior of different phases in complex CLs. They contribute to furnishing reliable relations between structure, transport properties, and reactivity [107,108]. Despite an enormous number of phenomenological models, less effort was put into exploring effects of the microstructure of the CL on transport and reactivity. Advanced experimental and theoretical tools can address the correlation of transport-reaction processes with structural details at meso-to-micro- and down to atomistic scale. Coarse-grained (CG) molecular simulation techniques can describe the system at the micro-to-meso level, while still being able to capture the morphology at long time and length scales [109]. The application of CG models, however, requires special care. One should note that due to the reduced number of degrees of freedom, CG simulations may not be able to accurately predict physical properties that directly rely upon time correlation functions (e.g., diffusion).

A significant number of mesoscale computational approaches has been employed to understand the phase-segregated morphology and transport properties of water-swollen Nafion® membranes [88,109–111]. Because of computational limitations, full atomistic models are not able to probe the random morphology of these systems. However, as demonstrated by these simulations and applications to other random composite media, mesoscale models are computationally feasible to capture their morphology. Several approaches have been used, such as termed cellular automata and coarse-grained meso-dynamics based on self-consistent mean field theory. For Nafion®, most of these simulations support the idea that narrow water-filled channels and irregularly shaped, nanometer-size clusters of ionic head groups and water form the proton-conducting network that is embedded into the hydrophobic matrix. Structural complexity is even more pronounced in CLs, since they consist of a mixture of Nafion® ionomer, Pt clusters supported on carbon particles, solvent and water. Independent computational strategies are generally needed in order to simulate the microstructure formation in CLs. For instance, the structure of the ionomer-phase in CLs cannot be trivially inferred from that in membrane simulations, as there are distinct correlations between Nafion®, water

and carbon particles in CLs. The computational approach based on coarse-grained molecular dynamics (CGMD) simulations is developed in two major steps [109,112,113]. In the first step, Nafion® chains, water and hydronium molecules, other solvent molecules and carbon/Pt particles are replaced by corresponding spherical beads with pre-defined sub-nanoscopic length scale. In the second step, parameters of renormalized interaction energies between the distinct beads are specified. CGMD data can be used to parameterize microstructurally resolved models [85,113,114] of transport processes in PEMFC electrodes. However, the remaining challenges of this technique are their high computational cost and as well as the development of appropriate experimental analysis tools able to give different validation frames of the predicted microstructures.

### 2.3. Cell level

The high computational effort of simulations at micro- or meso-scale restricts the size of the model domain and time span simulated. This motivates the use of mathematically reduced macro-models allowing simulations on cell level. Consideration of transport on the macro scale offers the opportunity to optimize durability and performance of PEMFC, as harmful operating conditions for different components of a fuel cell can be identified. Fig. 3 shows the most relevant processes, which have to been taken into account for each component on the cell level. Typically, models of different complexity exist to describe each of these processes. In the following, we give an overview of models describing the whole single cell including all components. Afterwards models developed for each cell component will be reviewed in detail.

#### 2.3.1. Single cell models

Springer et al. [115] developed a one-dimensional steady-state model of a single PEM fuel cell. The novelty of this model lies in the experimental relationship which correlates the membrane water content, at a certain temperature, to the water vapor activity. However, the main limitations are related to: (i) the assumption of isothermal volumes, (ii) the water flow description, which does not take into account specific physical phenomena, such as surface tension and capillary flow, and (iii) the validity of the study limited to a 117 Nafion® membrane. The model has been developed considering water in vapor state, with the possibility to account for liquid water, but only finely dispersed.

Maggio et al. [116] presented a simple but innovative PEMFC model in which an original calculation of diffusion losses was proposed, based on the following assumptions: (i) one-dimensional, (ii) isothermal and (iii) steady-state. Particularly, they stated that the assumption of a constant gas porosity in the electrode diffusional layer hinders the identification of the real limiting current density $I_{lim}$ involved in the calculation of diffusion losses. This assumption is mainly motivated by the effect that partial flooding at cathode reduces oxygen transport. For this reason an innovative expression has been exploited to evaluate the limiting current density with respect to the models available in the literature: indeed, they proposed an empirical function of cell operating temperature, oxygen molar fraction at cathode side and effective electrode porosity related to electrode water content. From their simulation results, they proved the cell performance being strictly related to electrodes water content and membrane technology.

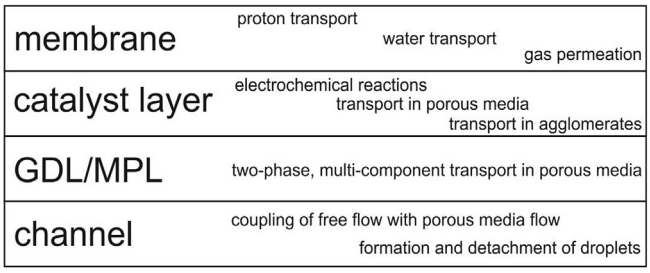


**Fig. 3.** Processes on the cell level which are relevant for PEMFC performance.

A similar approach has been chosen by Costamagna [117] who studied how to ensure proper membrane hydration and avoid local temperature peaks developing a three-dimensional PEM fuel cell model. A set of three-dimensional transport and balance equations has been defined to simulate the distribution of physico-chemical parameters, such as cathode and anode relative humidity, temperature and membrane water content. However, the main drawback of the approach applied in these two studies is that they neglect the presence of liquid water inside the porous media and at the interface between gas diffusion layer (GDL) and gas flow channel (GFC). This resulted in a less accurate representation of the real performance of the system. To overcome this limitation, Mazumder et al. [7] proposed a Computational Fluid Dynamics (CFD) model able to simulate liquid water transport inside a 3D PEMFC, observing that the assumption of no liquid water formation leads to an overestimation of the cell voltage, especially at high current densities. Instead, introducing liquid water transport mechanisms makes the model more accurate in predicting the cell polarization behavior.

Um et al. [118,119] developed a 3D computational fuel cell dynamics (CFCD) model of a PEMFC with a Nafion® 117 membrane. This model allows comparing the effects of straight and interdigitated flow fields on oxygen and vapor concentration at the cathode side and also on the current density distribution. The model embeds also a detailed Membrane Electrode Assembly (MEA) submodel where the membrane water content and catalyst layer reaction rate and ionic resistance are computed. Several assumptions have been made, e.g., constant cell temperature and that liquid water exists in the form of finely dispersed droplets (i.e. single phase hypothesis). The introduction of this latter assumption forced the authors to present the results as qualitative, due to the absence of a proper liquid water transport model. As a result, the authors stated that the interdigitated flow fields at the cathode side improved the cell performance at high current densities due to the enhanced mass transfer of the oxygen. Indeed, it has been observed that forced convection is the predominant transport mechanism rather than diffusion, improving liquid water removal (i.e. reduced flooding). Although the average current density is higher for interdigitated flow fields compared to straight flow fields, its distribution is much more non-uniform.

The model developed by Um et al. has been extended by Wang et al. [120,121] in order to simulate the transient processes occurring in a PEMFC due to a step change in the steady-state operating condition (i.e. current density or the level of reactant humidification). The authors developed a single-channel PEMFC model considering Gore® 18 μm and Nafion® 112 membranes to highlight the correlations between transient responses in terms of cell voltage and water content variation at low reactant humidity. From this study, the two main observations are: on the one hand, the ohmic resistance has been identified as predominant on the cell performance; on the other hand, membrane water content has been recognized as the chief part of the water management during transient maneuvers. Furthermore, it has been observed that at low reactant humidity the voltage transients exhibit an "undershoot" which increases with increasing current step change. Lastly, the authors stated that the exploitation of simplified models or lumped parameters could hinder the representation of such features.

*2.3.2. Membrane*

Recently, a large number of materials are tested for use as electrolyte in a fuel cell. These are, among many others, sulfonated hydrocarbon polymers (e.g. PEEK), phosphoric acid doped polybenzimidazole (PBI), polymer–inorganic composite membranes or solid acid membranes [122]. However, the most important and popular materials studied are perfluorinated polymers. Therefore, in this section we will start with a discussion of models describing the water sorption of perfluorosulfonic acid (PFSA) membranes, followed by a review on transport models for this type of material.

*2.3.2.1. Sorption models.* The aim of sorption models is to determine the water concentration inside the membrane. This concentration is conveniently expressed as the unitless quantity λ which is defined as the number of water molecules per sulfonic acid site in the polymer and depends on the water activity in a vapor phase next to the membrane. Additionally, a complete model needs to explain the water sorption from an adjacent liquid phase as liquid water is formed in the cathode during fuel cell operation.

Theoretically, the sorption from a fully saturated vapor phase and a liquid phase should be the same as the activity of water in both phases is equal to 1. However, there is experimental evidence, that the water concentration in the membrane is considerably higher for equilibrium with a liquid phase [123]. This discrepancy is called Schroeder's paradox [124]. Whether the persistent Schroeder's paradox really exists, is under discussion since more recent experiments support its absence [125,126]. Schroeder's paradox may be observed even though it might not exist if a non-equilibrium state has been measured for the contact with water vapor at 100% relative humidity. In this case, the equilibration may take hours or even days [127,128] and stopping the experiment too early results in observation of lower water content. On the other hand, assuming the existence of the paradox, its absence may be observed, if the relative humidity close to 100% is not exactly controlled and liquid water condensates on the membrane surface [127]. As a result, equilibrium with a liquid phase would be measured and the paradox would not appear.

A proposed thermodynamic explanation for Schroeder's paradox is the existence of a so called van der Waals loop, i.e., a double root solution for the Gibbs stability criteria [123]. In this case two distinct equilibrium states satisfying the Gibbs stability criteria exist, resulting in bifurcation of the sorption isotherm curve above a certain activity. However, as pointed out by Freger [129], this would lead to swelling hysteresis, which was not observed experimentally.

If thermodynamic equilibrium between membrane and adjacent fluid phase can be assumed, an equilibrium sorption model is applicable. In this case, the water content of the membrane is related to water chemical potential outside the membrane. In the following, we review several equilibrium sorption models, which have been developed to explain Schroeder's paradox.

The first model presented here was developed by Choi and Datta [130] and further improved by Choi et al. [131]. It is based on Flory–Huggins theory for the water/polymer interactions, includes the internal swelling pressure due to water uptake and the formation of the primary hydration sheath on the sulfonic acid groups. Schroeder's paradox is explained by a Laplace pressure forming at the open mouths of the hydrophobic membrane pores when the membrane is in contact with water vapor. Upon contact with liquid water, the pressure is released, lowering the chemical potential of water in the membrane thus leading to further water uptake.

In contrast to the work presented above, Eikerling and Berg [132] argue that the existence of hydrophobic pores in the membrane is not reasonable. They assume perfect wetting of the membrane pores leading to reduced vapor pressure over the curved interfaces between pore water and vapor. This causes capillary condensation and it is argued that this process is governing water uptake for high water content while hydration of the sulfonic acid groups governs sorption for low values of λ. In their model, the water content is determined from thermal and chemical equilibrium and mechanic equilibrium between gas or liquid pressure outside the membrane pores and liquid, osmotic and elastic pressure inside the pores. An analytic expression for the wall charge density as function of swelling of a single pore is derived. Again, Schroeder's paradox is attributed to the lack of capillary pressure for liquid equilibrium, this time raising the internal pressure as the pores are hydrophilic, and described as a first-order phase transition inside the membrane. The model predicts insensitivity of water sorption on the gas pressure in accordance with experiments but small variations of the relative humidity cause large variations of internal pressure in the range of $10^2$ bars. Therefore, it is concluded that hydraulic flux is the prevalent mechanism of water transport in PEM.

In his model [127] Kreuer uses a Langmuir type expression for the chemical potential of water in the hydration shells around the sulfonic acid groups inside the membrane with a second expression for the chemical potential of the bulk water in the membrane. Both depend on the internal swelling pressure of the polymer which is determined from the storage modulus and is a function of the water content. Assuming equilibrium between these potentials and the chemical potential of an adjacent vapor phase, λ as a function of relative humidity and temperature is obtained. Up to a relative humidity of 65%, water sorption is found to be exothermal. At higher humidification, sorption proceeds endothermic. From the model, the heats of hydration for water molecules forming the hydration shell around the sulfonic acid groups are obtained and the internal pressure is estimated to be as high as 10 MPa. It is stated that this high internal pressure cannot be caused by the surface tension of the polymer since it is about three orders of magnitude too low. Therefore, the existence of an "extended" surface layer with higher elasticity than the bulk membrane is proposed. The surface layer can maintain a large internal pressure until contact with liquid water causes its rapid restructuring. This leads to a drop of the internal pressure, causing Schroeder's paradox.

Both, the model of Choi et al. [133] and the model of Eikerling and Berg [132] assume an open pore configuration on the membrane surface. However, such a system would tend to reduce the interfacial area between the liquid water and vapor by reorganization of the polymer, resulting in an energetically more favorable state [129]. The model of Kreuer does not rely on this assumption but further experiments are required to establish a physical and mathematical model accounting for the reorganization of the proposed surface layer.

The assumption of thermodynamic equilibrium between membrane and adjacent fluid fails if the gas relative humidity or liquid water content in the cell is changing fast, for example, under automotive conditions. In that case, the operating conditions may change within a few seconds while it could takes minutes or hours for the membrane to equilibrate. Therefore, a description of the water sorption and desorption kinetics is needed. This can be done by describing the flux of water into and out of the membrane using mass transfer coefficients which may depend on temperature, humidity and mechanical properties of the membrane [128,134–142]. These mass transfer coefficients are then multiplied with the deviation in water activity from the equilibrium state at the interfaces. In order to do so, the equilibrium water activity inside the membrane due to the conditions outside the membrane needs to be determined from an equilibrium sorption model.

In the studies mentioned above, it is shown that the processes of sorption and desorption have a strong impact on the water profiles inside the membrane. This indicates the need for physical models of the structure and the relevant transport- and reorgani-

zation processes at the membrane surface. For now mostly simple empirical functions for the mass transfer coefficients have been used.

*2.3.2.2. Transport models.* The macro-scale transport models for PFSA membranes presented in the literature can roughly be divided into three different approaches, being the chemical potential-, diffusion- and hydraulic models. They can be distinguished by the driving forces considered. The most general driving force for transport is the chemical potential. Dependent on its definition, the driving forces for diffusion (gradients of species concentration) and convection (pressure gradients) may be included.

Two early models for the transport of protons and water in the membrane were developed by Springer et al. [115] and Bernardi and Verbrugge [143,144]. Both are 1D, isothermal, stationary models based on dilute solution theory. Springer et al. [115] employed a diffusion coefficient for water transport, incorporated electro-osmotic drag, and accounted for non-uniform water content in the membrane. The model is suited for conditions when the membrane is equilibrated with water vapor but does not treat the liquid equilibrated case thoroughly. They concluded that water diffusion and electro osmosis may balance each other to a great extent and that water is flowing from the anode to the cathode.

Bernardi and Verbrugge [143,144] used the Nernst–Planck equation in combination with Schögl's equation [145] to model water transport in a uniformly, fully hydrated membrane in contact with liquid water. This hydraulic model incorporates pressure differences between anode and cathode. For low current density, the model predicts water transport from cathode to anode, while for high current density it is vice versa.

Another hydraulic model by Eikerling et al. [146] considers electro-osmotic drag for the transport of water in the membrane counterbalanced by Darcy flow. In addition to the Bernardi–Verbrugge-model, it considers the local dehydration of the membrane and the membrane permeability as a function of the water content is calculated using the Hagen–Poiseuille–Kozeny equation. For the conductivity a percolation-type dependence on the water content is considered. The model predicts a critical current at which the membrane gets dehydrated at the anode side and the conductivity drops dramatically. Optimal membrane hydration is predicted for anode humidification with high water removal rates at the cathode side or for higher cathode pressures and anode water removal. In this work, diffusive and convective transport models are compared to experimental results. It is concluded that diffusive models fail to reproduce the experimental data because membrane dehydration is overestimated.

The model by Fuller and Newman [147] uses Stefan–Maxwell equations derived from concentrated solution theory in combination with material balances for each species. It predicts higher membrane conductivity with increasing current, but is not capable to reproduce transport losses at high current density due to its single phase nature. In the simulated concurrent flow channel, there is a high net flux of water from anode to cathode near the inlet and a comparably small flux from cathode to anode near the end of the channel. This is due to variation of the local current density and the water concentration. In this model, the chemical potential acts as a general driving force for the transport. This concept has been adapted several times, for example in the model of Janssen [148]. Unlike in the diffusion- or hydraulic models, the chemical potential is not separated in this approach. Therefore, no specific transport mechanism is assumed and the formulation is kept general. This results in the flaw that pressure- and activity variations inside the membrane cannot be resolved.

Again based on [147], Weber and Newman developed a model [149] which represents a combination of the diffusive Springer [115]- and the convective Bernardi/Verbrugge [143,144]-model. For the vapor equilibrated membrane diffusive single-phase-transport through collapsed channels is assumed while for a liquid-equilibrated membrane pressure driven convective flow through expanded channels is considered [149]. Both transport modes may occur in parallel, due to a coexistence of both kinds of channels. The fraction of expanded channels is determined from a measured pore size distribution, a contact angle estimation and use of the Young Laplace equation. With this quantity, it is possible to continuously interpolate between the two transport modes, enabling the model to give a physical description of Schroeder's paradox [124]. For validation, the model is incorporated into a simple cell model [150].

The model of Fuller and Newman [147] was also adapted by Thampan et al. [151]. To incorporate the interactions between hydronium ions and polymer matrix they used the "dusty-fluid model" [152]. The interactions between the stationary polymer-"dust" and the liquid species result in frictional forces and consequently reduced diffusional velocity. In this model, in order to calculate the convective velocity, Schlögl's equation [145] was applied.

As shown by Fimrite et al. [153] this approach was erroneous as extra viscous forces are introduced and therefore the binary friction model, developed in Ref. [154], is the favorable approach. Consequently Fimrite et al. presented a new model [155] for transport and conductivity based on the binary friction model. Transport is modeled solving generalized Stefan–Maxwell equations with membrane hydration and potential as driving forces. In their work, a comparison of the order of magnitude of different driving forces elucidated that pressure gradients across the membrane may be neglected. The corresponding conductivity model is a reduction of the transport model, neglecting concentration gradients of water across the membrane and therefore the influence of water transport on the conductivity. However, the parameters for the transport- and conductivity model are the same. This allows direct determination of the transport parameters from conductivity measurements.

Baschuk and Li [156] also used generalized Stefan–Maxwell equations with potential and partial density of water in the electrolyte as driving forces combined with non-equilibrium thermodynamics. This approach enabled them to easily couple the transport through the membrane and the electrodes by employing a single domain approach.

Apart from the approaches used above, Choi, Jalani and Datta [131] presented a conductivity model, accounting for transport of protons via en masse diffusion, surface diffusion and Grotthuss mechanism. To describe the different transport mechanisms, the Nernst–Einstein– and Einstein–Smoluchowski equation were employed. The conductivity model is based on their thermodynamic sorption model [133] for Nafion® involving Flory–Huggins theory [157]. It forms a theoretical basis for proton conductivity in polymer electrolytes and the authors conclude that a high fraction of pore bulk water is essential for fast proton transport via the Grotthuss mechanism.

From the review presented in this section, it becomes clear, that modeling of water sorption and transport, being of utmost importance for the correct description of water management in fuel cells, is a task of high complexity. The kinetic sorption models critically depend on a good equilibrium model and both, transport and sorption are strongly interrelated. A consistent description of these phenomena has, to the authors' knowledge, not been achieved in any model published today.

### 2.3.3. Catalyst layers

There are two main aspects which have to be taken into account when modeling the catalyst layers of PEMFC.

i.) The transport of the reactants and products trough the porous electrode

ii.) The electrochemical reactions occurring within the catalyst layers, i.e., the oxygen reduction reaction at the cathode and the hydrogen oxidation reaction at the anode

In the following we discuss the modeling approaches for both of these aspects.

*2.3.3.1. Transport models.* The simplest way of describing the catalyst layers is to consider a thin interface between the membrane and the GDL [158]. This approach considers the Cathode Catalyst Layer (CCL) as an interface that consumes electrons and produces water, but does not consider transport phenomena within the CCL. Therefore, these models are not suitable for describing transport in the electrodes.

Macrohomogeneous models assume that all phases are homogeneously mixed. A generalized Darcy law is used to describe transport phenomena [159]. Currently, properties of the CL like contact angle, porosity, relative conductivities and permeability cannot be measured locally and might be different from the average properties that are used in the macrohomogeneous models. Therefore, macrohomogeneous models may lack accuracy. Moreover, in the majority of cases the dynamics of the electrochemical double layer is not taken into account. Consequently, this approach is not appropriate for the modeling of local phenomena inside the CL and should be limited to modeling the performance at cell level [160].

Although distinct agglomerates might not exist due to agglomeration of Pt/C during the fabrication process, the agglomerate approach for modeling is still interesting. Indeed, by introducing a way to modulate the current transfer density, it allows for better prediction [1]. Various models can be found in the literature [161–163].

Agglomerate models consider phenomena that happen within the agglomerate length scale. They are made of either spherical or cylindrical assemblies of C/Pt, surrounded by a thin film of Nafion®. Reactants are dissolved in the electrolyte surrounding the agglomerate, and inside the agglomerate. Thus, gradients of concentration and potential can occur within the agglomerates [164]. Electrochemistry modeling can be based on the Butler–Volmer equation (cf. Section 2.3.3.2), were the efficiency factor enables to account for the geometry while the Thiele modulus accounts for the ratio between reaction kinetics and reagents diffusion [165]. The models show that the thickness of Nafion® around the agglomerate is a key parameter and should be no more than a few nm to promote reagents diffusion towards the Pt [163].

Harvey et al. [165] compared the agglomerate model and the thin-film model and concluded that the agglomerate model is able to predict with accuracy all the domains of the polarization curves. They suggest that loss of performance at high current density should be attributed to the structure of the CCL, in addition to flooding in the cell.

Going further, ordered electrodes can be made of straight aligned carbon nanotubes (CNT) [166,167]. This approach is particularly interesting since it enhances gas diffusion properties and optimizes the catalyst utilization, which then improves overall cell performance. Moreover, these uniformly distributed and aligned carbon nanotubes electrodes are more resistant to electrochemical oxidation. Aligned carbon nanotubes have most recently been modeled by Hussain et al. [167]. Once corrected by the membrane overpotential and the mixed-electrode potential, their 3D model is in good agreement with polarization curves from the literature. According to the model, a 10 nm thick Nafion® film around the C/Pt nanotubes yields the best performances in term of polarization curve. Also, the simulation showed that the optimum distance between the CNTs is 50 nm, while optimum length of the CNTs is 5 µm.

Cetinbas et al. [168], proposed an original geometrical model of discrete Pt particles on carbon support. The results reveal that the discretely-distributed particle approach can capture diffusion losses due to particle interactions and that particle-level diffusion plays an important role in the global diffusion. Moreover, contrary to uniform-coverage models that are unable to capture the effect of Pt loading on the polarization curve, this particle model is also able to demonstrate the strong impact of Pt loading on the overall performance. Moreover, the authors demonstrate that performance at high current densities is increased when Pt particles are located at the periphery of the agglomerates, thanks to reduced diffusion limitations.

More recently, Direct Numerical Simulations (DNS) have been developed to investigate the influence of the structure of the CCL on transport properties [169,170]. This approach is focused on transport through the secondary pores. However, this approach requires knowing precisely the structure of the CCL, whereas only statistical parameters (like porosity) are usually accessible from experimental data. So reconstruction of the structure from these parameters is first needed and this step, in addition to not being trivial, may introduce additional errors. Also these models are monophasic and thus unable to consider flooding of CCL. Pore Network Modeling (PNM) is well adapted to two phase transport in porous media and was first used to model such transport in the GDL (cf. Section 2.3.4). El Hannach developed a porous network model (PNM) to calculate gas and liquid transport properties in the CCL, allowing to analyze the effect of local properties of the CCL on the two-phase transport mechanism [171]. It shows that Bruggeman correlations that are often used to correct the diffusion coefficients in the CCL over-estimate the diffusion coefficient. Also, with the parameters used for this work, the protonic transport through the CCL is limiting. Therefore, the CCL located at the membrane side is more active.

A microstructurally-resolved model of the PEMFC cathode has been recently developed by Strahl, Husar and Franco allowing to study the impact of the carbon morphology (pore size distribution) and operating temperature dynamics on the electrode hydratation dynamics and cell potential variation [172]. This model allows simulating the pore water filling dynamics, an aspect not treated by PNM approaches. This is relevant to tackle the preconditioning phase of PEMFCs, usually neglected in the models reported in the literature.

*2.3.3.2. Electrochemistry models.* As discussed in Sec. 2.1 the ORR is a complex multi-step mechanism, which is still subject of numerous investigations on the atomistic scale. On the cell level simplified descriptions of the electrochemical reactions are needed. Models of different complexity have been developed to describe the reaction kinetics. These models either rely on like Nernst and Butler–Volmer equations or on mechanistic approaches.

The Nernst and Butler Volmer approach is the most common and has been discussed for both the HOR and the ORR in a recent review from Weber et al. [1].

The Nernst law enables the calculation of the reverse potential ($E_{eq}$) depending on the activities of the reactant and products. Then the Butler–Volmer equation is used to calculate the faradic current as a function of the difference between the applied electrode potential and the reverse potential. This potential difference is called the overpotential, also noted $\eta$.

The Butler–Volmer equation was first demonstrated for a single step reaction involving the exchange of a single electron. Neither the HOR nor the ORR fulfills these conditions. However, it is possible to generalize the Butler–Volmer law so that it can describe the HOR and the ORR.

More precisely, the Butler Volmer equation consists of two exponential terms (4), each one dominating either in case of high oxidative or reductive current. In these current areas, the Butler–Volmer equation can be simplified and leads to the Tafel law. The

two exponential terms have only to be considered at low current.

$$I = A \cdot j_0 \cdot \left\{ \exp\left[ \frac{\alpha_a nF}{RT} (E - E_{eq}) \right] - \exp\left[ -\frac{\alpha_c nF}{RT} (E - E_{eq}) \right] \right\} \quad (4)$$

Mann et al. [173] gave recommendations regarding the applicability of this equation for each case studied. The main advantage is that only a single reversible potential is considered, that can be obtained from experimental data. However, the elementary reaction steps are not modeled separately in this approach, which means that the coverages of the intermediate species on the catalyst surface are not calculated. This simplification becomes problematic as soon as the effect of the surface coverages is relevant, e.g., when studying the effect of catalyst contamination. A review on the effects of fuel cell contamination has been presented by Cheng et al. [174].

In contrast to the simple Butler–Volmer approach, mechanistic approaches describe the electrochemical reactions by multiple steps, e.g., adsorption of the reactants followed by oxidation/reduction steps and finally desorption of the product species. Thus, these models incorporate the evolution of intermediate species on the catalyst surface. These models are able to describe the complex behavior of the ORR more accurately, e.g., the change of Tafel slope on Pt(111) due to altering reaction pathways [175]. This approach also allows to include the effect of impurities, contamination and degradation mechanisms into the cell model [176,177]. However, in order to derive a realistic mechanistic model, the activation energies for all the elementary steps are required. These activation energies have to be obtained from heavy DFT calculations or from fitting to experimental data.

One example for such a mechanistic model is the double trap model proposed by Wang et al. [178]. This model describes the ORR by four reaction steps forming two reaction pathways and including the two intermediate species *O and *OH. The model allows describing the experimentally observed change of the ORR Tafel slope, which is not possible with a simple Butler–Volmer approach.

### 2.3.4. Gas diffusion layer (GDL)

Diffusion layers are called GDL (Gas Diffusion layer) and MPL (Micro Porous Layer). The GDL aims at distributing gas from the channels of the bipolar plates to the catalyst layer, removing the generated water and conducting the electrons to the bipolar plate ribs. The GDL is made of carbon fibers covered with polytetrafluoroethylene (PTFE) to increase its hydrophobicity, thus promoting removal of liquid water from the GDL. The MPL aims at improving water management [179–181].

For proper performance of the cell, the membrane has to be well hydrated. Depending on the cell temperature and on the current delivered, liquid water is present in the GDL. Consequently, two phase transport occurs in the GDL.

Within the GDL, it is now well established [182] that there is a strong coupling between thermal and water management, especially at high humidification of the feed gases, both being paramount for the performance of the fuel cell.

Djilali et al. [183] first demonstrated by modeling that the temperature and pressure gradients between the plates and the electrode are important and strongly affect the transport of water.

Weber et al. [182] then explained by a non-isothermal 1D model that the water is evaporated near the catalyst layer and condensates near the plate where the temperature can be several degrees lower. This transport of water decreases the flux of reactant gas from the channel to the catalyst layer.

Thomas et al. [184] presented an accurate experimental work to show the strong influence of the temperature profile on the water transport. They showed that water fluxes are linked to the thermal gradients that depend on the temperature difference between the catalyst layer and the plates. Concerning the MPL, Andisheh-Tadbir et al. [185] recently developed an analytical model for the thermal conductivity of the MPL depending on the pore size distribution, porosity, and compression pressure. After validation with experimental data, the model was used to find the optimal MPL structure with respect to mass and heat transfer.

In the following, we discuss three methods which have been established to study two phase transport in the GDL: Continuum Models (CM), Lattice Boltzmann models (LBM) and Pore Network models (PNM).

Continuum models consider a continuum media with (volume) averaged properties. They rely on generalized Darcy's law and phenomenological relationships [186]. However, due to the lack of length scale separation between the pore sizes (about 50 μm) and the thickness of the GDL (about 300 μm), CM can lead to inaccurate conclusions and are not appropriate to study of the GDL in detail [187].

Chun et al. [188] developed a 1D continuum model of the cathode GDL, based on the mass and momentum balance equations for conservation of water and oxygen, to optimize parameters of the GDL. Water removal and gas transport are strongly affected by the contact angle between liquid water and carbon GDL material, which depends on the PTFE content of the GDL. The authors showed that at low current density, the overall performance of the cell is not significantly affected by liquid saturation. Indeed, both reactant fluxes and water production are low. However, at high current density the higher the contact angle, the higher the water removal due to the increasing capillary forces. Consequently the gas transport increases, and so the overall cell performance is improved. Finally, the authors demonstrated that cell performance decreases with increasing GDL thickness, mostly due to decreased gas transport. Their conclusions are in good agreement with experimental observations.

Diffusion coefficients in the GDL are often corrected by a Bruggeman correlation for the porosity. Also, other corrections can be found in the literature and are reviewed in a recent paper from Zamel et al. [189]. The corrected diffusion coefficients are shown to be usually overestimated compared to experimental values. This review also provides state-of-the art values and analytical relations to be considered for modeling the transport properties in the PEMFC.

Pore Network Modeling is a powerful approach that enables to compute transport parameters in the GDL, to be then used in macroscopic models. PNM relies on capillary forces to describe liquid water invasion. Then both transport properties and electrochemical processes are computed after each step of invasion [171]. The network is made of a distribution of pores connected through throats. Effective transport properties are computed from both structural information (porosity, pore size distribution) and from physicochemical properties (wettability). Length scale separation (i.e. the existence of a representative elementary volume) is not met in the GDL and this is the reason why continuous models often fail in describing transport in the GDL with accuracy [187]. In this paper, the authors also underline that the injection conditions play a major role in the transport through the GDL, and more representative injection boundary conditions should be investigated. PNM enables a two phase modeling where evaporation and condensation (GDL are usually cooler than CL) are also taken into account. A thorny problem with PNM remains the injection condition [187]. Clearly, the injection condition plays a major role in the liquid water transport in the GDL. However this condition is closely linked to both water production and transport in the CL and transport through the MPL. This makes the injection condition difficult to determine. PNM is powerful in calculating transport properties in a region of mixed wettability. It was also shown that the through-plane diffusion coefficient of water decreases when the GDL's hydrophilicity increases

which is due to that pores are more and more the filled with liquid water [190].

The MPL is added to the GDL to promote water management. Meantime, oxygen diffusion remains efficient through the MPL. Zhang et al. as well as Ma et al. coupled pore network modeling and tomography to investigate the transport through the MPL [191,192]. They showed that the highly hydrophobic MPL with pores of a few tens of nm must have developed cracks, otherwise it would be impossible for the water to permeate. These cracks are the dominant pathways for the liquid water to go from the CL to the GDL. These results suggest that a multi-scale model of the MPL including both the pore scale and the cracks is worth developing.

In recent years, another methodology to simulate the properties in porous structures has been developed, the Lattice Boltzmann method (LBM). Originally, LBM simulated the motion of fluids by particles moving and colliding on a regular lattice, an artificial grid structure with lattice points having well-defined properties. Contrary to the Molecular Dynamics method which aims at tracking the movement of individual molecules, LBM simulations consider a collection of particles, each one may consist of multiple molecules. Consequently the computational load is reduced when modeling macroscopic flow in porous media. Moreover, LBM are highly versatile and numerically stable and the employed algorithm is inherently parallel in computation. LBM is well adapted when simulating flow to take into account complex geometries of the porous media structure, enabling, e.g., to consider the real morphology of the porous layers of the GDL. Doormaal and Pharoah have used a single-phase LBM to determine the permeability in a random GDL which had been generated using a Monte Carlo method. They found that the fiber structure of the GDL results in an anisotropic permeability. LBM has been found to be particularly relevant for multiphase flows in porous media where interfacial dynamics play a major role [193]. Many different aspects of two-phase transport in the GDL have been considered using the LBM: Niu et al. [194] presented a multiphase multiple-relaxation-time LBM to simulate the water–gas transport in the GDL. Based on these simulations they calculated the absolute and relative permeabilities in the GDL. Tabe et al. [195] used a 2D two-phase LBM to simulate the transport through GDL and channel, showing that the wettability of the channel strongly affects the two-phase flow. Koido et al. [196] have used a 3D two-phase LBM to derive empirical equations for the permeabilities of the liquid and gas phase in a carbon-fiber paper GDL. These empirical equations were then included into a macroscopic multiphase mixture model to investigate the two-phase multi-component transport in this GDL. Han and Meng [197] and Kim et al. [198] presented 2D multi-phase LBMs to investigate the liquid water transport through MPL and GDL. The simulations demonstrate the importance of the MPL on the water management in PEMFCs. Han end Meng also pointed out that large perforated pores are beneficial for fast liquid water removal. The impact of PTFE distribution in the GDL was studied by Molaeimanesh and Akbari [199]. A 2D multiphase multicomponent LBM was used in order to investigate the droplet removal from GDLs with different PTFE distributions. They observed that already small regions of uncoated carbon fibers can significantly hinder the droplet removal. In a following publication [200] the same authors presented a 3D LBM of the PEMFC cathode which takes into account the microstructure of the GDL and electrochemical reactions in the catalyst layer. The model includes multi-component transport but only for a single phase. Simulations comparing different GDL structures revealed that the orientation of the carbon fibers affects the current density distribution. An orientation of the fibers normal to the CL was observed to lead to higher current density variations and overall lower current densities.

Recently, García-Salaberri et al. [201] presented a methodology using a D3Q7 single relaxation time LBM in order to derive the effective gas diffusivity of a GDL depending on its local saturation and local porosity. The obtained effective diffusivity shows an anisotropic dependence on local porosity while the dependence on the local saturation was shown to be almost isotropic. In addition, 1D global averaging rules where introduced in order to obtain the global effective diffusivity from the local correlations.

#### 2.3.5. Interface between gas diffusion layer and gas flow channel

The two-phase flow over the interface between porous GDL and channel is an important and challenging aspect for PEMFC modeling. Several authors focused on the liquid water impact on the PEMFC behavior, investigating the effect of the operating conditions and the cell components characteristics on the liquid water removal, particularly at the cathode. Some authors coupled experimental activity and model analysis [202–207], whereas others exploit only experimental data available in literature to validate the developed mathematical models [208–210].

Kumbur et al. [205] modeled the detachment of single droplet, sitting on the Gas Diffusion Layer (GDL)/Gas Flow Channel (GFC) interface of a PEMFC, through a lumped static force balance. They also built a non-reactive cell experimental apparatus to support and validate their model. Through the proposed model and the experimental results, the authors developed an empirical relation between surface tension and PTFE content of the diffusion media. Furthermore, they also investigated the effects of channel height, PTFE content and gas flow velocity on water droplet contact angle hysteresis, observing that the water removal is eased by higher PTFE content and air speed and lower channel height. However, their focus was only on the understanding of the interaction between single water droplet and air flow, without analyzing water droplets dynamics (i.e. oscillation) and the whole system behavior (i.e. effects of water breakthrough and operating condition changes).

Following the same approach, Chen et al. [202] and Theodorakakos et al. [206] also analyzed in details this behavior. On the one hand, Chen studied the instability and detachment of a single droplet, due to air flow in the viscous regime, modeling a static force balance between the droplet and the shear flow. The investigation entailed two different droplet shapes, with spherical and cylindrical symmetry respectively, deriving a relationship for the drag and surface tension forces. They concluded that the water removal can be enhanced by increasing the GDL/GFC interface hydrophobicity, the GFC length or the air flow speed, or by decreasing the contact angle hysteresis or the GFC height. The results have been validated by means of experimental data and higher order models simulation results. On the other hand, Theodorakakos et al. [206] built an in-house non-reactive GFC to study the detachment of a water droplet from a porous media due to air drag, pointing out that the droplet formation and detachment are the main processes characterizing the water removal from the GDL/GFC interface. The modeling activity resulted in a CFD model of the droplet deformation, based on the Volume of Fluid (VOF) approach, whereas, a dedicated experimental activity has been performed in parallel, during which, oscillation phenomena have also been observed.

On the same line Chen et al. [202] and Cho et al. [203,204] developed an analytical model of a water droplet deformation and detachment from GDL surface accounting for both a 3D (sphere shape) and a 2D case (cylindrical shape). The simulation results are validated against experimental and numerical data (i.e. higher order models). An ad hoc non-reactive channel has been built to visualize droplets deformation and detachment through a Charge Coupled Device (CCD) camera. The main outcomes highlighted that water droplets removal is improved by decreasing channels height or increasing surface hydrophobicity (e.g. PTFE content), channel length and gas speed.

Among others, He et al. [209] investigated the influence of several parameters, such as critical droplet size, contact angle, surface tension and GDL mean pore size, on the water removal in the cell. They developed a Two-Fluid (TF) model for the representation of the PEMFC two-phase flow, with particular attention of the phenomena occurring at the GDL/GFC interface. The obtained results, validated through a comparison with the experimental data of Wang et al. [211], pointed out that a high contact angle and a low surface tension ease water removal.

Interesting observations were made by Mortazavi et al. [212], who investigated the effect of different polytetrafluoroethylene (PTFE) content in the GDL on water droplet emerging and detachment. They build an ex-situ direct visualization apparatus directly fed with air or hydrogen, in order to understand the influence of the gas species on the two aforementioned mechanisms. They observed that the droplets breakthrough location is usually constant and their detachment is enhanced by increasing the gas flow and/or increasing the PTFE content. Moreover, they also observed that aged GDL show uniform contact angles, without having any impact on droplet detachment.

Some publications exploit the Volume of Fluid (VOF) method for the mathematical model development, as done by Chen [208], who developed a 3D model of a droplet deformation and detachment from the GDL/GFC interface exposed to an air flow. The model is mainly based on a static balance between air drag force and droplet surface tension, which highlights the dependence of droplet detachment size, air velocity, contact angle and channel height. The validation procedure is performed exploiting experimental data available in the literature [206,207], in parallel with a parametric study to show the influence of the design parameters on droplet detachment. Throughout the simulation results of the proposed model, Chen showed that the air velocity at detachment has an inverse relation to the 2/3 power of the droplet size. Moreover, as observed by other authors [202–204,213], water droplets removal is enhanced by more hydrophobic surfaces, higher air velocity and lower channel height.

Another approach, based on the Mean Value Model (MVM), has been followed by Esposito et al. [214,215] to investigate the liquid water transport mechanisms at the cathode. The authors developed a low order model to simulate the capillary driven liquid water transport through the GDL. Furthermore, they also implemented a sub-model for the simulation of droplets formation at the GDL/GFC interface. This model allows the evaluation of the water accumulated at the cathode with the estimation of the effective GDL saturation and the water droplet occupation at the GDL/GFC interface. An in-depth experimental investigation of the effects of droplet oscillation behavior on its detachment characteristics has also been performed [216] by building a non-reactive channel to capture pictures of a single droplet emerging at a specific location during its growth and at the detachment using a CCD camera. The novelty of their work resides in the image post-processing procedure, which allows the observation of droplet oscillation behavior induced by air shear flow and the definition of an explicit correlation between critical droplet size and air velocity. They also highlighted the importance of the oscillation mechanism on droplet detachment.

Based on the observation by Esposito et al., the mathematical model of Polverino et al. [210] describes the main influence of the oscillation mechanism on the droplet detachment by means of a dynamic lumped force balance among drag, surface tension and inertia. The model has been validated through the exploitation of experimental data available in the literature [206], showing good agreement with the experimental results. Moreover, a parametric study has been performed in order to underline the influence on air flow, channel height and static contact angle on droplet detachment diameter.

### 2.4. Stack and system level

In order to obtain the required amount of voltage, in real applications fuel cells are piled up into stacks. In the literature it is usual to find the stacks modeled multiplying the effect of one cell by the number of cells [217]. However, there exist differences between the cells of a stack. Mainly, temperature and distribution of reactant gases may vary fom one cell to another depending on the position of the cell in the stack. As a consequence, the formation of liquid water depends on the cell position, too. These characteristics affect not only the performance but also the degradation of the cells. Indeed, some works present CFD stack models showing pressure and temperature changes from one cell to another. In Ref. [218] the temperature profile from cell to cell is analyzed and its influence on the output voltage of individual cells shown to be significant. In Ref. [219] a CFD model of a 72-cells stack is used to analyze the best configurations and channel dimensions for a uniform distribution.

Moreover, in order to be able to produce energy, it is necessary to integrate the fuel cell stack with other components to form a fuel cell-based power generation system. A generic scheme showing the interrelation between the main components of the power generation system is presented in Fig. 4.

Fuel cell system modeling has played a decisive role in system design and developing, as well as in the optimization and testing of fuel cell control strategies. Since the control strategy for a real system has to take into account important actuator and peripheral system dynamics, the cell level model has to be upgraded to make it suitable for the controller design. However, modeling and controlling PEM fuel cell based systems is a particularly challenging task due to the interactions between physical phenomena of different nature and scale and the presence of nonlinear structures.

Although most physical phenomena occurring in a PEM fuel cell system can be incorporated in the macroscopic CFD models at cell level, it leads to time-consuming simulations with high computational costs. To improve performance and durability of fuel cell systems, the design of controllers that optimize these aspects under all the expected operating conditions is required, and the design of good controllers is highly dependent on the available dynamic models. Therefore, the task of obtaining control-oriented models at system level has become important. Control-oriented PEM fuel cell stack and system modeling has been studied by several authors using different approaches.

A dynamic PEMFC model specifically developed for control engineering was presented by Pukrushpan et al. [217] to study two main control problems: (i) the amount of oxygen supplied at the cathode side to the fuel cell system and (ii) the hydrogen flow supplied at the anode side and provided by a fuel processor system. The model describes the transient behavior of the air compressor, the manifold filling–emptying dynamics, the reactant partial pressures and the membrane humidity level. However, the model neglects the electrochemical reaction kinetics and stack temperature is treated as a constant parameter due to its slow time constant. Concerning the air flow control at stack inlet, the authors found that the use of stack voltage as feedback signal increases the observability of the system; moreover, they observed a tradeoff between fast air flow regulation and electric power delivery, which can be eased by using an auxiliary battery or super-capacitor. The results obtained addressing the hydrogen flow control showed that the hydrogen molar fraction regulation strongly depends on the valve commands during load transients. The model is shown to be suitable for the evaluation of features and properties of different control configurations such as dynamic feedforward, observer feedback, and proportional plus integral controllers. The work points out that regardless of the selected controller, there is a dynamic limitation due to the fact that the compressor uses part of the stack power to ac-

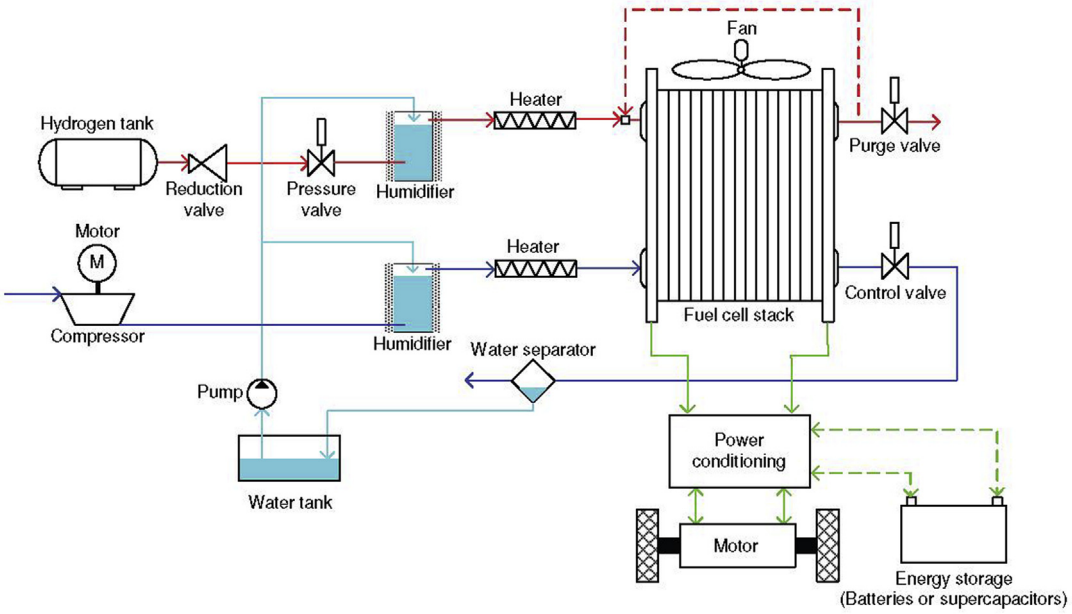


**Fig. 4.** Schematic of a fuel cell system.

celerate. This results in a necessary trade off between fast regulation of the oxygen excess ratio and fast delivery of the desired net power during transient operations.

A similar approach can be found in the works of Miotti et al. [220] and Arsie et al. [221,222], who exploited a lumped modeling methodology to develop a PEMFC system model oriented towards automotive applications. More in detail, Miotti et al. [220] proposed a lumped isothermal model of a pressurized PEMFC system aimed at automotive applications, without considering the presence of water in liquid state. The model is based on a filling–emptying approach and takes into account several components, such as stack, air compressor, supply and return manifolds and heat exchangers. The authors exploited a 1D and a 1 + 1D model to develop multidimensional look-up tables in order to simulate the net water flux across the membrane and the profile of water content along the electrolyte. From the simulation results, they stated that, even though more realistic results have been obtained exploiting the 1 + 1D maps rather than the 1D maps, the membrane water content and, in turn, the voltage performance do not vary substantially. The study performed by Arsie et al. [221,222] deals with understanding the optimal control strategy to be adopted for a hybrid vehicle based on PEMFC, aiming at enhancing the system efficiency. The authors focus on the energy flows among the powertrain components (i.e. fuel cell, battery pack, electric motor, etc.), exploiting a lumped model in which gray-box parameters and black-box models are embedded. Analysis based on this model quantifies the system efficiency increase gained by the introduction of a rate limiter on the stack power. Moreover, a multilevel control strategy has been proposed, through which the energy flows and the control logics are managed. The obtained results proposed control strategies useful to investigate the system behavior in different scenarios and also in severe transient conditions. Moreover, through the proposed approach a good tradeoff among fuel consumption, system performance and safe operation can be found, with respect to an optimized strategy for fuel-cell hybrid vehicles.

Within all the different dynamic stack and system modeling, a very important task is to develop models that can be integrated into the controller in order to compute the control action. These models are normally linearized, low order models which permit to keep the computation time within the control period. In the last decade, several control strategies based on internal models have been reported for the control of hydrogen consumption or oxygen stoichiometry of PEM fuel cell systems [223–225]. As an example, Talj et al. [223] proposed a model of a PEMFC air subsystem for control strategies design, to which an order reduction approach was applied, downgrading from a fourth-order to a third-order model, with a relative error of maximum 5%. On the same line, Zhang et al. [225] proposed an adaptive control strategy to act on the air flow at a PEM cathode side to keep at a certain level the excess of air. This approach aims at reducing the air starvation during fuel cell operation. The authors underlined the needs for a suitable and precise definition of system nonlinearities and timevarying features, which can compromise the optimal system operation. While the advanced control strategies perform properly in a large range of operating conditions, their control objectives remain in the reactants feeding domain. After suitable solutions were found for these control objectives, an important effort has been done to improve heat and water distribution inside the fuel cell. Thus, models and controllers that take system humidification, air flow supply, water distribution and membrane water dynamics into account have been proposed and can be considered for the development of suitable control strategies [222–226]. All these controller internal models are lumped parameter models and thus, they assume homogeneous conditions (not profiles) of the internal variables along the different stack directions. In the case of water distribution, this is an important limitation as CFD models show significant differences from one point to another [7]. These differences may cause stronger degradation in cells close to the endplates compared to internal cells and also increased degradation in the outlet zones compared to the inlet zones [227]. Kunusch et al. [228] developed a dynamic multi-input multi-output (MIMO) model by linear identification of the system time constants on an experimental laboratory fuel cell system under a specific operating condition. The two inputs are fuel cell stack current and cathode mass flow rate and the outputs are fuel cell stack voltage and cathode pressure. The resulting model can be used either for model-based control design or for on-line analysis and error detection. Based on this initial model, Kunusch et al. [229] developed a control-oriented, non-linear model that simulates the most typical features of a laboratory PEM fuel cell system through ordinary differential equations (ODE), primarily focused on

the reactant gas dynamics. The methodology used to develop the model is based on a modular procedure, combining theoretical modeling techniques and empirical analysis. The obtained model is fully experimentally validated and can be easily adapted to other systems because its parameters maintain their physical meaning.

Since energy conversion, storage and transportation become more and more important, especially for stationary fuel cell systems, fuel cell models have been upgraded to account for the added system dynamics. The incorporation of energy storage elements into the fuel cell system and the analysis of electrical topologies and power management have been addressed [230,231]. Other works consider complementary energy sources such as photovoltaic panels or wind turbines [232].

However, the results of these studies are limited because either they use an electrochemical model that is not experimentally validated or experimental models that do not take into account the electrochemistry. Moreover, these models do not consider the performance losses due to liquid water or degradation effects. More research is needed to combine these effects not only in CFD modeling but also control-oriented modeling, considering mitigation strategies for degradation mechanisms and water management related performance improvement.

### 2.5. Coupling between the scales

Two approaches are possible to develop multiscale models of electrochemical power generators: the direct one and the indirect one [233–235].

Direct multiparadigm multiscale models consist in coupling "on-the-fly" models developed in the frame of different paradigms. For example, continuum equations describing transport phenomena of multiple reactants in a porous electrode can be coupled with Mean Field (MF) theory or kinetic Monte Carlo (kMC) simulations describing electrochemical reactions among these reactants. However, as has been established [236,237] kMC is the only approach able to describe the adspecies surface transport and lateral interaction and reaction. Several numerical techniques are well established to develop such a type of models applied in the simulation of physicochemical processes, e.g., catalytic and electro-deposition processes [94,100,238]. In the field of catalysis, KMC simulations have been used to calculate instantaneous kinetic reaction rates on a catalyst calculated iteratively from concentrations in turn calculated from CFD-like continuum transport models [89]. Computationally speaking, these direct multiparadigm methods are very expensive; therefore, the indirect multiparadigm method represents a feasible alternative. This method consists in extracting data from a lower-scale and using it as input for the upper-scale via their parameters. For example, activation barriers for elementary reaction steps can be extracted from DFT by Nudged Elastic Band (NEB) calculations [239], and then injected into Eyring's expressions to estimate the kinetic parameters

$$k_i = f_i \frac{k_B T}{h} \exp\left(\frac{-E_i}{k_B T}\right), \tag{5}$$

where $f$ refers to the frequency pre-factor, $k_B$ and R the Boltzmann and universal gas constants, T the absolute temperature and $h$ the Planck constant. These expressions are used for the calculation of the individual reaction rates $v_i$ at the continuum level [51].

$$v_i = k_i \prod_y a_y^{\nu} - k_{-i} \prod_{y'} a_{y'}^{\nu'}, \tag{6}$$

where $a_y$ and $a_{y'}$ refer to the activity of respectively the reactant $y$ and product $y'$ and their stoichiometry coefficients, $\nu$ and $\nu'$ while $k_i$ is rate constants for the forward reaction and $k_{-i}$ is that of the corresponding backward reaction. Eq. (6) is in turn used for the calculation of the evolution of the surface or volume concentrations of the reaction intermediates, reactants and products, following

$$K_n \frac{da_y}{dt} = \sum_i \nu_i - \sum_j \nu_j, \tag{7}$$

with $K_n$ being the number of reaction sites per mol of reactant.

The NEB method yields the minimal energy paths (MEP) between given initial and final states. The method consists in linearly interpolating a set of images between the known initial and final states, and then minimizing the energy of this string of images. Each "image" corresponds to a specific geometry of the atoms on their way from the initial to the final state, a snapshot along the reaction path. Thus, once the energy of this string of images has been minimized, the pathway corresponding to the minimum in energy is found. A more accurate value of the MEP can be obtained with the Adaptive Nudged Elastic Band method [240], where a zoom in the transition state (TS) is made by changing the initial and the final state by two NEB states closer to the TS.

Another example of multi-paradigm model is the use of Coarse Grained Molecular Dynamics (CGMD) for the calculation of the materials structural properties (e.g. tortuosity $\tau$ and porosity $\varepsilon$) as function of the materials chemistry, which are used in turn for the estimation of the effective diffusion coefficient used in continuum reactants transport models [241].

$$D_{eff} = \frac{\varepsilon}{\tau} D_0, \tag{8}$$

with $D_0$, the molecular (binary) diffusion coefficient of the diffusing species, e.g., hydrogen–vapor water mixture at the anode or air–water vapor mixture at the cathode. Thanks to this approach $D_{eff}$ can be estimated on-the-fly in terms of the chemical composition and may be updated during the multiscale simulation [242].

In this way one could then imagine building up an electrochemical power generator model with macroscopic equations based on material parameters extracted from atomistic and molecular level calculations. Within this sense, in 2002, Franco has invented the multiscale simulation package of PEMFC called "MEMEPhys" [112,243]. The model is an indirect multi-paradigm, multiscale approach: a continuum model describing electrochemical and transport mechanisms with parameters extracted from ab initio databases (for the reactions kinetic parameters as function of catalyst chemistry and morphology) and CGMD calculations (for the materials structural properties as function of their chemistry). More recently the simulation package MS LIBER-T (*Multiscale Simulator of Lithium Ion Batteries and Electrochemical Reactor Technologies*) has emerged [85,244,245]. It is programmed in C and Python and designed to support direct multiparadigm calculations, for instance, simulations coupling on the fly the numerical resolution of continuum models (e.g. describing charge transport in the electrode volume) with discrete models (e.g. Monte Carlo module describing the elementary reaction kinetics [88]). Another novelty introduced by MS LIBER-T is its capability of integrating phase field models describing phase formation, separation and evolution, mechanisms highly relevant for material microstructure simulations [233].

Another multiscale modeling framework written in C/C++ is DENIS (Detailed Electrochemistry and Numerical Impedance Simulation) [246,247], which allows for modeling of SOFC (solid oxide fuel cell), PEMFC and DMFC (direct methanol fuel cell) as well as several types of batteries. DENIS provides complex electrochemical models on the scale of the catalyst surface as well as two-phase, multi-component transport on the cell level.

Within the presented multiscale frameworks elementary kinetic models for the oxygen reduction reaction based on DFT calculations have been developed [51,175], giving insight into the relevant

reaction pathways and surface coverages over the full range of cathode potentials.

Considering the coupling to higher scales, stack and system modeling, as well as single cell modeling, are in the macroscopic CFD domain. However, if they have to include all the cells and system elements, CFD models become very large, and thus, slow. In the case of model-based controllers, simulation time needs to be faster than real time. As a consequence, models of reduced order that maintain the relevant input–output dynamic relationships are required. The application of model order reduction techniques to fuel cells has been analyzed in the literature [248].

## 3. Modeling degradation mechanism in PEMFC

### 3.1. Membrane

Deterioration of PFSA membrane properties such as gas separation, proton conductivity and electrical insulation is governed by thermal, mechanical and (electro-) chemical degradation [249]. This section gives a short overview of the different effects on the membrane and their impact on fuel cell performance and lifetime followed by state-of-the-art modeling approaches to describe these degradation processes.

#### 3.1.1. Thermal degradation

Under standard fuel cell conditions (~80 °C), the effect of thermally induced degradation of the electrolyte is assumed insignificant [250]. However, after heating Nafion® films to 95 °C cross-linking of sulfonic end-groups was observed [251] causing reduced conductivity. The maximum operating temperature for Nafion®-based membranes is about 100 °C which is below the glass transition temperature of the material of 110 °C. Above this temperature dissociation of ionic clusters [252] and increasing crystallinity [253] of the membrane were found.

Contrary to elevated temperatures, fuel cells in automotive applications are also required to resist repeated exposure to temperatures as low as –40 °C which can cause the formation and melting of ice. In freeze/thaw cycle tests reduced fuel cell performance and lifetime was observed when studying the influence on the membrane properties [254]. Dry Nafion® 112 membranes were exposed to 385 cycles between –40 °C and 80 °C. While no visible sign of deterioration, delamination or tearing was found, a dramatic decrease in elongation at failure, lower ultimate strength and density has been observed. Also, a reduction of the anisotropy of material properties in machine and cross direction, like dimensional changes due to swelling and tensile strength was stated. Repeated freezing and thawing caused reduced oxygen permeability. Based on these observations, it was suggested that rearrangement of the sulfonic groups was responsible for the changes in the material properties.

It can be stated, that thermal degradation is negligible when close to standard operating conditions. To the authors' best knowledge, no cell-scale modeling work focusing on thermal degradation of the membrane in PEMFC has been done so far. Further, the effects of subzero conditions on the membrane have been investigated but are not understood in depth and detail, which motivates the development of models on lower length scales.

#### 3.1.2. Mechanical degradation

Ex-situ analysis of aged membranes reveals several features of degradation like crazes, cracks, pin-holes, thinning and elongation of the membrane [255]. The formation of these defects is partly caused by cyclic stress resulting from repeated swelling and shrinking of the membrane due to water sorption and desorption [256–258]. As a consequence, the electric contact between MEA and electrodes may be reduced and the cross-over of gases increases. This leads to lower OCV (open circuit voltage) [259], higher ohmic losses and therefore to reduced performance of the fuel cell. With increasing cross-over of reactants, local hot-spots may develop which in turn accelerate the degradation. Finally, this causes catastrophic failure of the membrane.

On the modeling front Weber and Newman were the first to investigate the influence of a constrained membrane [260]. The model predicts reduced water content in a constraint membrane. It is shown that compression improves the flux of water from cathode to anode under all humidity conditions due to increased liquid pressure at the cathode and reduction of the membrane thickness. Hence, it was concluded that the effect of constraint should not be ignored.

Accordingly, constitutive models describing the mechanical behavior of the membrane were developed. These models are able to describe the stress–strain behavior of the polymer under varying strain rates, temperatures and humidity conditions [261–265]. The same has been done for an ePTFE reinforced membrane [266]. It was concluded that the residual in-plane stresses can be reduced significantly by introduction of a reinforcement layer. Humidity cycles led to cyclic mechanical loads which in turn led to hysteresis in the stress–strain behavior of the membrane. A constitutive model capturing this behavior was presented [264]. For a membrane in contact with liquid water the stress–strain behavior changes considerably just like the water uptake of the membrane changes when exposed to water vapor or liquid water (Schroeder's paradox). A membrane in contact with liquid water will exhibit the rubbery behavior of an elastomer, which has been modeled in another study [265].

Based on these constitutive relationships, finite element models have been developed to calculate the distribution of stresses inside the membrane [257,266–269]. For this purpose, most often the commercial software package ABAQUS [270] is used. From the resulting stress distribution, regions prone to mechanical degradation can be identified. However, the challenging task to create a model capable of predicting the failure of the membrane due to crack or pin-hole formation, and therefore the lifetime of the membrane, remains.

A more practical approach has been adopted in Ref. [271] where stress vs. cycles-to-failure curves were fitted to data of dynamic mechanical analysis experiments. Relating the stress to the change of the relative humidity during one cycle allows prediction of the cycles-to-failure depending on the operating conditions. However, stress vs. cycles-to-failure curves give no insight on the degradation processes and lack physical meaning.

A model able to predict the mechanical degradation of a membrane has recently been presented by Burlatsky et al. [272]. In this model, in order to account for the non-linear viscoelasticity of the material, the molecular theory proposed by Eyring [273], which was initially developed to describe the mechanical properties of textiles, is extended allowing prediction of stress relaxation in a constrained polymer. Additionally to this constitutive model, three model components to predict the lifetime of a GORE-SELECT membrane were used. The first model component is used to calculate the transient behavior of the relative humidity (RH) distribution in the gas channels as a function of the operation conditions, cf. Ref. [274]. Secondly, a stress model is used to calculate the stress distribution in the membrane for a given RH profile. Finally, based on the calculated stress, the membrane lifetime is predicted using the damage accrual model which is based on fitting model parameters to data from dynamic mechanical analysis (DMA) experiments, resembling the procedure given in Ref. [271].

Kusoglu and Weber [275] presented a model for the mechanical degradation of the fuel cell membrane, describing the growth of pinholes during load cycling. The model describes the plastic deformation and stresses caused by the swelling during humidity cycling. Based on the model, tensile stresses and the plastic strain increment have been identified as relevant factors for the pinhole growth and the effect of operating conditions and model param-

eters have been studied. Furthermore, the model was combined with a simple empirical model for the chemical degradation. The predicted hydrogen crossover was shown to be in rather good agreement with experimental data. However, as discussed by the authors, mechanical and chemical degradation can accelerate each other and therefore their contribution on the membrane aging cannot be separated easily. Thus, model improvements are still necessary to take into account these synergetic effects more accurately.

Today, state-of-the-art constitutive models are able to describe the transient behavior of the mechanical membrane properties depending on parameters like temperature, humidity and strain rate. With the help of stress distribution models, high stress regions in the membrane can be identified and operating conditions to decrease these stresses can be derived. However, the formation of crazes, cracks and pin-holes in the membrane strongly depends on the presence of defects in it. The mechanisms which locally initiate an individual crack or pin-hole have not been clearly identified and may not be resolved on the macro-scale either. Therefore, no modeling of pinhole formation and crack evolution has been performed on the cell level so far. The mechanical degradation of the membrane plays an important role in the overall degradation of the cell, although it is proposed that chemical degradation is more severe for the membrane [276–278]. Further developments on experimental setups to investigate the interplay of mechanical and chemical degradation are indeed required.

### 3.1.3. Chemical degradation

Chemical degradation covers the effects of membrane decomposition due to (electro-) chemical reactions and membrane contamination. Contaminants like fuel impurities, air pollutants and cationic ions can poison catalysts, increase protonic membrane and catalyst layer resistance or degrade the catalyst layer structure and hydrophobicity. These effects are reviewed elsewhere [174,279].

It is common agreement that, during fuel cell operation, the production of hydrogen peroxide $H_2O_2$ and subsequent decomposition to radical species is the main cause for chemical membrane degradation [280–283]. However, reports on the location of membrane degradation are contradictory: Degradation was observed at the anode [284,285] or at the cathode [286,287]. Also the role of a platinum band, which may form during operation due to catalyst degradation, is still under discussion. In Refs. [288,289] higher degradation is attributed to the presence of a Pt band while in Ref. [290] the contrary is reported. Subsequent investigations found that membrane degradation decreases with increasing Pt particle density in the membrane [291–293].

It is proposed that $H_2O_2$ is formed at the electrolyte electrode interfaces by reaction of cross-over gases on the Pt-particles [285,294,295]. According to Ref. [280], $H_2O_2$ has a diffusion length in the millimeter range. Therefore, the location of $H_2O_2$-formation and membrane degradation are not necessarily coupled. $H_2O_2$ may form at the anode with $O_2$ crossing the membrane or as a side product of the ORR on the cathode side. Both ways of $H_2O_2$ formation are discussed in Ref. [283] but it is stated that the predominant mechanisms remain unclear.

When $H_2O_2$ is decomposed, $HO^{\bullet}$ and $HOO^{\bullet}$ radicals are formed which in turn attack the electrolyte material. Inside the membrane, this decomposition is catalyzed by metallic impurities [296] or Pt-particles from the catalyst layers [255].

For the attack on the polymer structure, several sites have been proposed. Some of the polymer backbones terminate in H-containing end groups which have been identified to be a weak spot and a mechanism for the attack on these sites has been proposed [297]. This mechanism causes an advanced unzipping of the backbone accompanied by the release of HF and $CO_2$. When such unzipping reaches a junction of the backbone and a side chain including sulfonic acid sites, the whole side chain is “cut off” and forms the so-called “molecule A” which can be found as a degradation product in the effluent water of the cell [298]. This loss of sulfonic acid sites leads to a reduction in membrane conductivity. Fluorination of the weak end groups resulted in greatly reduced fluoride emission rates (FER), and therefore enhanced chemical stability [297].

Also, the scission of polymer side-chains has been proposed as a degradation pathway [299]. This cutting of the side chain causes further degradation via unzipping until a junction of side chain and backbone is reached. Then, two weak end groups on the backbone are produced leading to an irreversible increase in weak sites and therefore accelerated chemical degradation. In Ref. [300], it was proposed that at high humidity degradation is governed by the unzipping mechanism and under low humidity conditions scission of the side chains dominates. The exact location for radical attack on the side chain is under debate. Sulfonic acid sites as well as ether linkages have been proposed [300–303].

For the modeling of chemical membrane degradation, two types of models have been developed. To gain insight in the basic mechanisms of degradation and to interpret experimental results, kinetic 0D (zero dimensional) models are applied [280,281,299,300]. Further, 1D models for chemical degradation of the membrane were embedded in a simulated fuel cell environment [282,283].

A kinetic model to determine the contribution of backbone unzipping and side chain cleavage to the overall chemical degradation process in various degradation environments was developed by Xie and Hayden [299]. A relationship for the fluorine fractional loss, the concentration of carboxylic acid in the membrane and the ratio of rate constants for side chain cleavage and unzipping were derived. Correlation of infrared spectroscopy measurements to this kinetic model gives the basis to determine the rate constants ratio under different experimental conditions. This model allows for the prediction of the influence of the polymer structure on the degradation mechanisms, therefore giving guidance for improved chemical durability through meaningful molecular design.

Chen and Fuller conducted durability tests at different temperatures and degradation was studied at anode, cathode and in the center of the membrane using X-ray photoelectron spectroscopy (XPS) and HF/TFA ratio analysis [281]. Degradation was accelerated at higher temperatures and was found to be more severe on the anode side. Decomposition of the polymer backbone and side chains was also reported. Degradation in the bulk of the membrane was observed to be slow and mainly due to backbone decomposition. This was attributed to attack of molecular oxygen on carbon centered radical end group on the main polymer chain at low temperatures. To investigate the influence of the different mechanisms and explain the experimental results, a kinetic model was developed. In this model, four steps of membrane degradation are proposed: (1) radical formation via Fenton’s reaction, (2) reaction of $O_2$ with carbon centered radicals located on the backbones and backbone unzipping due to $HO^{\bullet}$ attack, (3) termination of unzipping by reaction of two carbon centered radicals which again form a stable backbone structure and (4) side group degradation. Assuming steady state, an expression for HF formation is formulated allowing for a qualitative explanation of the experimental results. Based on this expression, a rate expression for fluorine loss is derived taking into account the contributions of Fenton’s- and side group degradation reaction. They concluded that degradation accelerates with higher temperature, and that it is more severe at the anode due to higher $H_2O_2$ and radical concentrations. In the bulk membrane, they observed that backbone decomposition outweighs degradation via the side chains and they found that $O_2$ attack on long chain radicals contributes to the membrane degradation.

The kinetic models of Gubler et al. [280] to the one of Ghelichi et al. [304] both aim at determining the chemical degradation resulting from $H_2O_2$ decomposition via Fenton’s chemistry and subsequent radical attack on the polymer. Both start from a similar

set of chemical reactions. While Gubler et al. use rate constants valid for room temperature only, Ghelichi et al. also give the activation energies enabling their model to determine degradation at fuel cell operating conditions. After comparison of the different reaction rates, Ghelichi et al. discard the reaction of $Fe^{2+}$ with $OH^{\bullet}$ because the $OH^{\bullet}$ concentration is low and the direct formation of $OH^{\bullet}$ from $H_2O_2$ because the reaction is negligibly slow. Gubler et al. consider reactions involving $H_2$ and $O_2$ which occur in the membrane due to gas cross over. Comparison of the reaction rates shows that these reactions are kinetically relevant and cannot be neglected as was done in Ref. [304]. Therefore, the results of Ghelichi et al. are only valid for ex situ Fenton's tests and not for in situ fuel cell operation. Assuming constant Fe and $H_2O_2$ concentrations, Ghelichi et al. derive an analytic solution for the calculation of the OH radical concentration enabling direct calculation of the FER without the need to consider the HOO radicals in the system explicitly. One flaw of this analytic solution is that the attack of the radicals on the polymer does not influence the steady state concentration of $OH^{\bullet}$. In Ref. [280] Gubler et al. show that radical attack on the polymer reduces the $OH^{\bullet}$ steady state concentration up to two orders of magnitude, depending on the iron content, which suggests that the model of Ghelichi et al. overestimates the $OH^{\bullet}$ concentration. The model of Gubler et al. neglects radical attack on the side chains while the Ghelichi model incorporates the mechanism with the coarse-grained consideration of the polymer structure. Thus, even though both models give valuable insights into the mechanisms of chemical degradation, due to the assumptions and simplifications mentioned above, the models cannot be applied to predict membrane degradation under fuel cell operating conditions.

Concerning the 1D models, Kundu et al. investigated degradation of a Gore™ PRIMERA® series 5510 catalyst coated membrane [286]. To increase mechanical stability, the membrane contains a layer which is reinforced with ePTFE (expanded polytetrafluoroethylene). The MEA was tested under OCV conditions. Scanning electron microscopy (SEM) revealed membrane degradation at the cathode and a platinum band in the membrane was observed. A semi-mechanistic 1D transient model was developed and compared to the experimental investigation of fluoride emission rate (FER), crossover current and OCV. In this model, degradation is assumed to start at the cathode and to advance in a wavelike manner to the anode causing thinning of the membrane. Crossover current, $H_2O_2$-formation, subsequent radical formation and membrane degradation is proposed to depend on the flux of $H_2$ from anode to cathode. The $H_2O_2$ formation from oxygen cross over is neglected in this model. The loss of electrochemical active surface area is incorporated and equations are solved using the 'method of lines'. Cumulative fluoride release of anode and cathode, crossover current and the evolution of OCV are simulated. It is concluded that all fluoride emissions result from ionomer degradation next to the cathode. Further, degradation is assumed to advance to the reinforcement layer. When the degradation front reaches the ePTFE layer, the fluoride generation slows down as the reinforcement is assumed inert. The lower anode FER is attributed to the larger diffusion resistance when fluoride is generated at the cathode and needs to cross the membrane.

A 1D fuel cell model incorporating chemical degradation of the membrane was presented by Shah, Ralph and Walsh [283]. It is based on the solution of conservation equations for mass, charge and energy including a detailed description of the transport phenomena in different layers of the fuel cell. A sub-model describes $H_2O_2$ formation, evolution of radicals from Fenton's reaction and direct formation at the anode. Chemical degradation is assumed to proceed via unzipping of the backbone, side chain cleavage and decomposition of "molecule A". Model results are concentration profiles of the considered species and their evolution with time. These results suggest that degradation propagates from the anode to the cathode. Therefore, it is concluded that FER measurements alone are not sufficient to determine the main location for degradation as the process is time-dependent, localized and diffusion effectively distributes HF in the membrane. The influence of oxygen concentration at OCV, membrane thickness, load operation, temperature, water activity and reaction rate constants was investigated.

A second 1D continuum model was developed by Gumalla et al. [282] where the model domain consists of the membrane and the electrodes. Diffusive transport and reaction of crossover gases, radical formation and attack on the membrane with subsequent HF release under OCV conditions is incorporated into the model. The resulting reaction diffusion equations are solved using a central finite difference scheme and a nonlinear solver implemented in software package gPROMS [305]. Radicals can be formed and quenched at Pt-particles which are assumed to be uniformly distributed inside the membrane. This assumption is due to an earlier study [306] where, in contrast to other experiments, no platinum band was observed, but a homogeneous distribution of Pt particles was found in the membrane. A general reaction of hydroxyl radicals with Nafion® is incorporated but no specific degradation mechanism is assumed. The model results are fitted to the measured FERs data from the OCV-tests conducted in Ref. [306]. OH radicals are assumed to be produced directly by partial oxygen reduction on the Pt particles in the membrane. Influence of the Pt-particle size and the spacing between them, concentration of oxygen at the cathode, relative humidity and membrane thickness on the degradation rate was simulated. It is found that the FER strongly depends on the particle size as the quenching of produced radicals is more likely on bigger particles. The spacing between particles determines whether radical formation is controlled by diffusion or the reaction kinetics. For small distances between particles, radical generation takes place in a narrow region where $H_2$ and $O_2$ are almost completely consumed while for larger spacing, $H_2$ and $O_2$ concentrations are higher throughout the membrane and radical production takes place in the whole membrane. Variations of the relative humidity influence degradation is three ways: (1) decreasing RH increases the oxygen molar fraction in the supply gases, (2) decreasing RH decreases the gas permeability and (3) higher membrane hydration influences the hydration shell of the Pt particles, reducing the available surface area for radical generation. This leads to an increase in degradation up to a RH of approximately 0.2–0.4, for higher RH, the FER decreases again.

The first model to incorporate the effect of chemical degradation on the macroscopic properties of the membrane was developed by Coulon et al. [307,308]. In Ref. [307], an elementary kinetic model is presented simulating $H_2O_2$ formation at the anode, $OH^{\bullet}$ formation via Fenton's reaction and radical attack which leads to side chain cleavage and loss of sulfonic acid sites. It couples a new model for the membrane to the multiscale electrode models [77,83] of MEMEPhys® [80,309]. For the membrane, the conductivity model presented in Ref. [131] is extended resulting in an equation for the conductivity depending on chemical degradation. For the first time, a feedback between chemical degradation and the transport properties of the membrane is established. They concluded that membrane degradation has a pronounced effect on the fuel cell performance above 1000 h of operation. Cell current and membrane thickness have only minor influence on the increase in specific membrane resistance.

Recently, Wong and Kjeang developed a model for simulation of in-situ chemical degradation [310] They consider $H_2O_2$ formation via two-electron-transfer at the anode and radical formation from a single Fenton's reaction of $H_2O_2$ with $Fe^{2+}$. The radical attack on the polymer structure starts at the side chains with attack on the ether bond of the $\alpha OCF_2$ group. Unzipping along the side chain leads to an intermediate oxygen centered radical and further degradation results in main chain scission with the formation of two

carboxylic acid groups on the polymer backbone. From there, the degradation proceeds via unzipping along the backbone. This degradation model is incorporated into a 1D, single phase transport model in the GDLs, MPLs and CLs of the cell with electron transport through the solid phase. In the catalyst layers and the membrane, an equation is solved for the electrolyte potential and transport of water, $H_2O_2$, $H_2$ and $O_2$ is simulated and additional transport of degradation products and hydroxyl radicals is modeled in the membrane. Evolution of the polymer structure, dry membrane thickness, evolution of the membrane ionic resistance and cell open circuit voltage are simulated and the model is validated against experimental results [311]. In a following work [312] the model is expanded to incorporate the transport of $Fe^{2+}$ and $Fe^{3+}$ in the catalyst layers and the membrane and the redox cycle of these ions. Radical formation strongly depends on the presence of $H_2O_2$ and $Fe^{2+}$. The total iron ion concentration in this model is kept constant and the electrochemical reduction of $Fe^{3+}$ to $Fe^{2+}$ is incorporated in the catalyst layers. This reaction, as well as $H_2O_2$ formation is strongly dependent on the electrode potentials. Therefore, cell operation at three different voltages is simulated: OCV, 0.9 V and 0.7 V. At OCV, the concentrations of $H_2O_2$ and $Fe^{2+}$ are high at the anode side causing severe degradation. At 0.9 V, the $H_2O_2$ concentration remains almost the same, while the degradation rate is found to be reduced by 57%. This reduction is caused by the lower $Fe^{2+}$ concentration at 0.9 V which demonstrates the high impact of the state of iron on the degradation rates. At 0.7 V, the ionomer potential gradient increases resulting in an almost zero net flux of $Fe^{3+}$ to the anode which reduces the $Fe^{2+}$ formation there. Iron ions accumulate at the cathode resulting in degradation at the cathode side under higher load conditions. Overall, the degradation at 0.7 V is reduced to one tenth.

### 3.2. Catalyst layer

Degradation of the catalyst layers fall into two categories. One category is where cell aging impacts on cell durability such as platinum dissolution and particle coarsening as well as carbon support corrosion described below. The other category, not described here, is related to ice formation in the different layers of the MEA, for example, during cold start or under prolonged cell exposure to subzero temperatures which has an immediate often catastrophic impact on cell performance. In this section, the modeling approaches to describe the degradation mechanisms within the catalyst layer are reviewed.

#### 3.2.1. Platinum dissolution

The stability of the platinum catalyst is crucial for fuel cell durability. However, typical PEMFC conditions, i.e., low pH, high temperature and potential cycling, are known to promote platinum dissolution [313,314]. Several models have been developed to describe this degradation mechanism.

Darling and Meyers [315] proposed a model for platinum dissolution and movement in the MEA that claims to fit reasonably well with experimental data from literature. The model takes into account three electrochemical reactions involved in platinum dissolution. Kinetic parameters are provided for the different steps. Later, the authors [316] also proposed a model for the movement of the dissolved platinum in the ionomer in the catalyst layer and in the membrane. Bi and Fuller [317] proposed a similar model that includes also the formation of a Pt band in the membrane, but it appears that the model does not predict Pt degradation rate very well, which leads to the conclusion that additional mechanisms are involved, such as nanoparticle coarsening.

More recently, Ahluwalia et al. investigated the role of oxide coverage and particle size on the stability of carbon supported Platinum nanoparticles [318]. Rotating Ring Disk Experiments were carried out and models were developed to explain the results. As only Pt dissolution occurs in such a configuration ($Pt^{2+}$ ions are removed in the electrolyte and do not contribute to the growth of other particles by Ostwald Ripening), only Pt dissolution is modeled. A solid solution theory was formulated to model the variation of the Pt dissolution rate with the potential, the oxide coverage and the size of the particle. They were thus capable of explaining the peak in the dissolved $Pt^{2+}$ concentration at about 1.1 V that is observed in Rotating Ring Disk Electrodes. Indeed, high potentials promote Pt dissolution but also the formation of platinum oxides. The oxide coverage increases, reaching unity at 1.1 V, and protects the Pt from dissolution. Their kinetic model shows that this competitive balance governs the Pt degradation at high voltage. The simulations were found to be consistent with experimental results for the Pt dissolution rate. Most of the existing dissolution models include the effect of oxide coverage by taking into account that the formation of a protective oxide layer reduces the platinum dissolution as discussed before. According to these models, under cycling conditions dissolution mainly occurs during the anodic potential sweep of potential cycling, since the protective oxide layer has been reduced at low potential [318]. However, recent experiments [319,320] suggest that the effect of platinum oxides on the dissolution is more complex. According to these experiments the dissolution is mainly caused by the place-exchange of PtO during the reduction of the oxides, i.e., dissolution occurs mainly during the cathodic potential sweep in contrast to the predictions of the previously mentioned models. Thus, model improvements are necessary in order to correctly describe platinum dissolution under transient operating conditions.

In order to achieve this goal not only the correlation between the formation and reduction of platinum oxides and the platinum dissolution has to be taken into account, but also the oxide formation kinetics has to be modeled properly. Even though platinum oxides have already been studied for more than 40 years, both experimentally [321] and theoretically [322], an accurate mathematical model to describe the formation and reduction of the oxides under transient operating conditions remains a challenge. Recently, Redmond et al. [323] presented an innovative model which describes the oxide coverage by means of oxide distributions on the edge and on the planar sites of the platinum particles. By performing CV simulations, the model was shown to be able to correctly reproduce the shape of the CVs for varying scan rates and varying upper potential limits. However, as pointed out by the authors the potentiostatic oxide coverage growth rate predicted by the model was much lower than experimentally observed. Thus, model improvements are still necessary.

The models discussed above consider pure platinum catalysts only. However, understanding the degradation mechanisms of Pt-based bimetallic catalysts is also important as these materials generally provide higher activity than pure Pt towards the ORR and are devoted to be one of the favorite cathode catalysts. A multiscale mechanistic model (including transport at the MEA level and local insight in the electrochemical double layer, EDL) has been developed by Franco et al., [76] for Pt–Co catalyst performance and degradation rate estimation. The model allows ranking the degradation rate among Pt–Co, $Pt_3Co$, Pt and $PtCo_3$ catalysts depending on the cell operating conditions. The model shows that the catalyst durability depends on the catalyst stoichiometry with the lowest stability being obtained for $PtCo_3$. The model also predicts that $Pt_3Co$ offers the best activity, even compared to Pt in good agreement with experimental data, and pointing out that the nanostructural properties of the catalyst and overall PEMFC operation conditions are of paramount importance towards the optimization of bimetallic catalyst nanoparticles activity and durability.

*3.2.2. Coarsening and coalescence*

Experimentally, it is well known that during aging, the catalyst surface area first exhibits a fast decrease but then tends to stabilize. This stabilization is related to a growth of the average platinum particle size and cannot be described by simple dissolution models described before. Under fuel cell working conditions, nanoparticles tend to sinter or agglomerate on the support [324]. The understanding of the underlying mechanisms of sintering and Pt degradation, including dissolution in acidic media [319,325], is paramount to improve the durability of a fuel cell. At the atomic level, two different mechanisms might occur:

i) Ostwald ripening, a process in which a large nanoparticle grows by atoms that are dissolved from smaller nanoparticles;
ii) the coalescence of small nanoparticles into a larger one [326]. The stability of a nanoparticle on a support is influenced by a large number of parameters: temperature, pressure, electrochemical environment, the strength of the interaction between the metal and the support, and the strength of the metal–metal bond in the presence of the adsorbates [35,324]. DFT calculations show that the formation of Pd clusters on a support surface depends on a delicate interplay between the metal–metal bond strength and the metal-support interaction [327]. On an atomistic level, reactant-assisted Ostwald ripening will occur in the presence of strong interactions between the metal surface and the reactants [328].

Previously, the Ostwald ripening mechanism was described in details in Ref. [329]. The driving force is the difference in the electrochemical potential between particles of various sizes. Indeed, the chemical potential depends particularly on the size of the particles: the bigger the particles, the smaller the chemical potential according to Gibbs–Thomson energy that links the radius of the particles and the chemical potential of the Pt inside. Electrochemical Ostwald ripening that occurs in PEMFC both involves transport of $Pt^{2+}$ in the electrolyte and transport of electrons in the carbon support: led by the difference in the chemical potential of two close Pt particles, $Pt^{2+}$ ions dissolve from the smaller particle and precipitate on the larger one. Simultaneously, electrons are transported via the carbon support from the smaller particle to the larger one. Consequently, a voltage appears between Pt nano particles and bulk particles. It was experimentally validated that this voltage decreases with time, demonstrating that the average radius of the nano particles increases. Parthasarathy and Vikar reported on Ostwald ripening of Pt nanoparticles deposited on large carbon surfaces that leads to nanoparticles coarsening [330].

On the other hand, the coalescence mechanism is based on the movement of the platinum particles on the support surface. If two particles collide they can coalesce, thus forming a larger one. This mechanism is expected to be promoted by the presence of liquid water in the catalyst layers and proposed to be responsible for loss of active catalyst surface at low potentials, where Ostwald ripening is negligible [331]. However, even though the coalescence mechanism has been discussed already for a long time [332], its relevance for the overall catalyst degradation in PEMFC still remains unclear, since experimental measurements of the ECSA loss do not allow to distinguish between Ostwald ripening and coalescence as underlying mechanism. A possible distinction between both mechanisms is by ex situ analysis of the particle shapes and the particle size distribution (PSD), since the evolution of the PSD is very different for both mechanisms. Numerically, modeling the coalescence mechanism is much more challenging compared to the Ostwald ripening process, since the coalescence mechanism requires solving integro-differential equations for the PSD [333]. Most of the catalyst degradation models in the literature consider Ostwald ripening as the only mechanism. However, recently, Ahluwalia et al. [334] presented a model which includes both mechanisms, Ostwald ripening and coalescence. They pointed out that in principle the experimentally observed particle growth could also be reproduced using a model without coalescence. However, as stated by the authors this would require an increase of the dissolution kinetics by two orders of magnitude, which was argued to be inconsistent with previously reported dissolution kinetics.

Pt dissolution or growth due to Ostwald ripening has been modeled by Holby et al. [335]. The authors used a Butler–Volmer like equation where an additional term accounting for the size-dependant stability is introduced, thanks to the Gibbs–Thomson energy. The Ostwald ripening mechanism was coupled to the formation of a Pt band in the membrane following H2 crossover. The simulated evolution of the particle size distribution was shown to be in good qualitative agreement with experimental data.

Recently, Li et al. [336] presented a 1D model for the platinum catalyst degradation taking into account Ostwald ripening and Pt dissolution–re-precipitation through the ionomer phase. They observed a non-uniform catalyst degradation caused by the crossover of $H_2$ and the consequent formation of a platinum band within the membrane. Based on the model they concluded that a thinning of the catalyst layer leads to an accelerated catalyst degradation, which might pose a problem when going to low platinum loading.

Urchaga et al. [337] presented a catalyst degradation model, which takes into account the particle growth due to Ostwald ripening, coalescence and detachment mechanisms. The platinum oxide formation is not modeled explicitly. The model was validated by fitting the ECSA losses obtained from various accelerated stress tests. Based on this analysis, the authors concluded that detachment only plays a role at high potentials where carbon corrosion occurs. However, as pointed out by the authors, the analysis did not allow for a clear distinction between the Ostwald ripening and coalescence mechanism. Therefore, further analysis is required to clarify the role of coalescence on the particle growth.

A model describing the coupling between electrochemical double layer effects, Pt dissolution and coarsening due to Ostwald ripening and associated particle size change kinetics was for the first time proposed in Ref. [338]. The incorporation of the EDL effects permitted the simulation of the feedback between the electrode potential and the Pt degradation kinetics, i.e., describing how the electrode performance impacts the Pt degradation kinetics and conversely how the Pt degradation kinetics impacts the performance decay.

*3.2.3. Carbon corrosion*

Carbon corrosion is of major concern for long-term durability of PEMFC. Carbon corrosion leads to reduced carbon support and Pt particles can detach from their support, agglomerate or become isolated. In addition, carbon corrosion can lead to a significant collapse and compaction of the CLs, thus blocking transport pathway for the reactant gas through the CLs. Moreover, carbon corrosion entails increase of hydrophilic properties of the support, thus promoting flooding of the electrodes [274]. Thus, carbon corrosion contributes to CL degradation through multiple mechanisms. Carbon corrosion mainly occurs at the cathode side during start-up and shutdown, when the cell can be subjected to local fuel starvation that induces in-plane currents [339].

Meyers and Darling [340] developed a mathematical model for the carbon corrosion in PEMFC. The model consists of a 1D representation of a single cell, describing the $H_2$ and $O_2$ concentrations along the channels as well as the electrolyte potential and the integrated current densities, i.e., the model does not resolve the distributions through the MEA. Butler–Volmer equations where used to describe the hydrogen and oxygen reactions while a Tafel expression with a Langmuir adsorption term was applied for the carbon corrosion reaction. The model shows how a maldistribution of hy-

drogen can lead to a reverse current in the fuelstarved region causing accelerated carbon corrosion. Furthermore, the effect of start/stop cycles on carbon corrosion was investigated. Based on the model, start procedures to mitigate carbon corrosion have been proposed.

Takeuchi et al. [341] developed a model for carbon corrosion that studies the influence of the operating conditions on the corrosion rate. Carbon corrosion is induced by oxygen and hydrogen coexistence at the anode due to oxygen crossover, especially during start-up and shutdown. During these phases, if there is no nitrogen purge, oxygen presence in the anode side induces reverse-current phenomena, even if there is no current drawn. It has been demonstrated that the corrosion current depends on the oxygen partial pressure at the anode. A similar model is proposed by Hu et al. [342]. It leads to the conclusion that the rate of carbon corrosion at the cathode side in the case of fuel starvation is strongly dependent on oxygen diffusion through the membrane. Experimentally, carbon corrosion has been observed in conjunction with disrupted membranes [343]. This is in good agreement with the assumption that the $O_2$ crossover is the root cause of carbon corrosion.

A multiscale model also including carbon corrosion has been developed by Franco et al. [85,112,243,245]. The model includes the description of the electrochemical double layer and takes into account multiple reaction steps. It is shown that carbon corrosion can favor platinum coarsening [80]. The simulations also suggest that an optimal operation conditions exist in order to mitigate degradation.

By combining Coarse Grain Molecular Dynamics generated databases and MEMEPhys model, Malek and Franco demonstrated that the structural properties of Nafion® can affect the carbon corrosion kinetics in the cathode catalyst layer [241]. Nafion® adsorbed on the carbon support was shown to reduce the carbon corrosion due to the hydrophobicity of the Nafion® backbone.

### 3.3. Gas diffusion layer

Among the various degradation mechanisms that lead to decreasing cell performance, degradation of the GDL plays a major role [344]. GDL are made of carbon fibers covered by a hydrophobic agent, usually PTFE. Consequently, degradation mechanisms can target the carbon and/or the PTFE. It could also modify the pore size itself by compaction of the structure. However, observations on a variation of the pore size are not consistent and will not be discussed here. Carbon oxidation requires the presence of a catalyst. However, as very little Pt is present in the GDL (some Pt can be accumulated at the GDL/MPL during aging due to platinum dissolution in the catalyst layer), this degradation mechanism is unlikely to occur.

Degradation is mainly caused by the loss of hydrophobicity due to PTFE degradation [255]. It is commonly stated that loss of hydrophobicity entails flooding of the GDL, leading to a decrease of cell performance. Several authors have investigated the effects of this loss of GDL hydrophobicity.

Pauchet et al. [345] have recently studied GDL degradation by achieving a one-way coupling between Pore Network Models (PNM) and Performance Model (PM). In their models, gas diffusion is calculated by PNM for various amounts of liquid water and then serves as input for the PM. Liquid water is supposed to increase the loss of hydrophobicity. Consequently, presence of liquid water plays a major role in cell performance degradation. Pauchet et al. showed that gas diffusion decreases when the fraction of hydrophilic pores increases. Also they demonstrate that the decrease of the gas diffusion is not linear and that a percolation threshold exists. Finally, loss of hydrophobicity of the gas diffusion layer can lead to cell performance losses comparable to the one observed experimentally. This suggests that degradation of the PTFE plays an important role in the overall degradation of the GDL.

Seidenberger et al. [346] developed 3D Monte Carlo model in order to investigate the effect of the PTFE degradation on the water distribution within the GDL. With decreasing the PTFE coverage from 85% to 65% a growth of the water clusters and an overall increase of water content within the GDL was observed. When further reducing the PTFE coverage to 55%, the simulation predicts a strong increase of water content and a consequent formation of a large cluster extending over the whole GDL. As pointed out by the authors, at this point a significant obstruction of the gas transport through the GDL has to be expected.

From a different point of view, an interesting analysis of the impact of water flooding on the diffusivity at cathode side is presented by Casalegno et al. [347]. They developed a simple 1D + 1D model of the steady state water transport through the GDL able to reproduce both water concentration and effective diffusivity for a GDL structure with and without an MPL. This model is based on isothermal domain and differential-algebraic systems describing water and air fluxes. The main outcome of this model consists in the definition of the GDL effective diffusivity as a function of a local flooding coefficient (representative of the flooding magnitude), temperature and water concentration. The results obtained with the model, in agreement with the data gathered during a dedicated experimental activity, highlight that the pore obstruction caused by flooding does strongly affect the GDL only without an MPL, whereas not much if the MPL is included, with consequent less fluctuation of water transport.

### 3.4. Bipolar plates

The bipolar plate (BPP) is an integral component of the fuel cell (FC) stack, which is used to interconnect single FC layers [348]. BPPs have several important functions for FC operation, such as, uniform fuel and oxidant distribution over the active areas, water and heat removal, current transport from cell to cell, and leak proofing of reactants and coolants. Physically, they constitute around 80% of the stack weight and 45% of the stack cost [348]. During FC operation, the BPPs are exposed to both oxidizing (at the cathode) and reducing (at the anode) conditions, which can result in oxide layer formation and corrosion of the constituent materials. Such conditions lead to a degradation of the BPP performance and eventually the stack performance [349]. Particularly, the interface between the BPP and the gas-diffusion layer (GDL) shows an interfacial contact resistance (ICR) that increases over time, the effects of which are increase in voltage drops, decrease in efficiency, and hence, decrease in output power.

In order to enhance the durability and life cycle of a BPP, detailed degradation analyses is required in order to identify and quantify the degradation mechanisms for constituent materials and interfacial interactions. There is a large body of experimental literature on BPP degradation via corrosion and contact resistance analysis [350]. There are various factors inherent to PEMFC operations that support BPP corrosion, including high humidity (presence of moisture), low pH due to acidic membrane, and elevated temperatures (as compared to “standard” environmental corrosion). Most importantly, as corrosion is an electrochemical process, it shows a strong interaction with electrochemical FC operation. At open cell voltage or low current densities, the cathode potential can reach >1 V, which for stainless steel (SS) is within the so-called “transpassive” region, leading to significant corrosive stress on the metallic BPPs. Under load, the anode potential, which shows a potential close to 0 V vs. reversible hydrogen electrode (RHE), approaches 100 mV, which lies in the so-called “active” region, leading again to high corrosive current. Also, during dynamic operation at startup and shutdown, the BPP can be forced to trans-passive or active regions [348].

Despite broad experimental evidence, a detailed theoretical approach towards understanding the various involved phenomena in BPP degradation is still missing. However, models would largely help towards a predictive analysis of the involved phenomena while economizing and optimizing relevant experimental setups. The pathway towards a BPP degradation model should be carried out in two steps, that is, (*i*) describe the physical origin of the interfacial contact resistance (without degradation) and (*ii*) include corrosion through protective oxide growth and metal dissolution.

Only few studies on numerical modeling of contact resistance between BPP and GDL exist. Zhou et al. [351] developed a microscale numerical model by considering the BPP surface topology, GDL structure, and clamping pressure and numerically determined the resistance for each contact spot. The total resistance was obtained by considering all contact spots as resistances in parallel and summing the results. Wu et al. [352] improved the mentioned contact resistance model by accounting for deformation of the carbon fibers present in the GDL and a rigid BPP asperity. They observed that the deformation of carbon fibers in GDL under clamping pressure leads to an increase in contact area between BPP and GDL and hence reduces the contact resistance. They also developed a regression model for the estimation of the contact force and contact area based on a normally distributed carbon fiber length and compression depth, and uniformly distributed contact spots between BPP and GDL. The proposed regression model was in good accordance with the experimental data. However, the accuracy of their models was reduced due to the simplifying assumption of frictionless contact between the carbon fibers in the GDL and BPP asperities. Mishra et al. [353] used a fractal-based model to predict the contact resistance between GDL and BPP and measured the contact resistance experimentally. The GDL surface roughness parameters, which were important inputs for the fractal model, could change during compression and hence are difficult to characterize. Zhang et al. [354] developed simple computational methods for estimating contact resistance between BPP and GDL based on experimentally obtained constitutive resistance–pressure relations. With the help of a semi-empirical model, they discussed the effect of assembly clamping pressure on the contact resistance between BPP and GDL. It was observed that the contact resistance is mostly influenced by the average value of the clamping pressure rather than its distribution. However, the effect of surface roughness was neglected in their model, which might influence the actual contact area between the BPP and the GDL. Also, their test pressure distribution was not representative of an actual flowfield distribution in the BPP, and hence did not account for the effects of a transient pressure variation in the flow field due to load cycling. We are not aware of models that include increase of interfacial contact resistance due to electrochemical degradation phenomena such as oxide formation on the metallic contact surfaces.

Corrosion itself is a well-understood process, and a large body of literature exists covers corrosion theory [355] and modeling [356]. However, the corrosion of the BPP itself has, to the best of our knowledge, not yet been modeled. Note this is a highly complex process owing to non-uniform FC operating conditions and non-linear dependence of the corrosion current on electrode polarization. However, corrosion models have been developed for other PEM fuel cell components, such as carbon corrosion [357] (see Sections 3.2 and 3.3). The knowledge and methodology gained from those studies could be extended to BPP corrosion, while considering the specific chemical environments of the BPP (oxidizing at the cathode side, reducing at the anode side).

### 3.5. Coupling of performance and degradation models

In his recent review [81], Franco underlines that in current PEMFC models, the instantaneous feedback between performance and aging is not described. They describe which operating conditions enhance a given degradation process (e.g. carbon corrosion) but do not describe the impact of this degradation process on the instantaneous performance (a prediction of the transient behavior of the PEMFC MEA electrochemical observables, such as the cell potential degradation or durability, is not provided). According to Franco, the main drawbacks of current PEMFC degradation models are:

- Aging mechanisms addressed in a separated (uncoupled) way: Most of the available kinetic models describing degradation phenomena in PEMFCs focus on Pt-based MEA, where Pt and carbon materials are treated as a single phase (no distinction between Pt and carbon phases).
- As in ex-situ experiments, each material aging phenomenon has been the subject of separate modeling studies. However, in real PEMFC environments, aging mechanisms of the different individual materials are expected to compete and to interact.
- Potentiostatic–potentiodynamic simulations: In most of the available kinetic degradation models, the Butler–Volmer electrode potential is the input variable, the output being a material corrosion rate and the cell current. Implicitly, it is assumed that the potential of the nanomaterials is equal to the external/macroscopic applied potential. Again, the cell potential evolution and the associated MEA durability cannot be predicted in this way. In fact, the majority of the single-cell tests available in the literature are made with current being the input variable.
- Use of the classical Butler–Volmer theory: This empirical theory, largely used in the PEMFC modeling community, describes electrochemical (electron transfer) reactions on ideal planar electrodes. The use of such a macroscopic Butler–Volmer theory cannot be really justified for describing electron transfer reactions on nanomaterials with an evolving structure (in fact, standard transition-state theory assumes that the 'catalyst' properties, following the definition of catalyst, are time-invariant or recover its morphology after reaction).

Franco et al. proposed several multiscale models to overcome some of these issues, including descriptions of coupled electrochemical aging processes (e.g. Pt and $Pt_xCo_y$ oxidation/dissolution/ripening, carbon catalyst support corrosion, PEM degradation) [81,86,90,212,273,275,293–296,285,297,298]. The approach describes the feedback between the instantaneous performance and the intrinsic material aging processes, thus durability of individual components and of the entire cell can be predicted. Within this context, the model has provided interesting information on the competition of aging phenomena, by demonstrating that anode contamination by CO can be used, under some particular current-cycle conditions, to mitigate cathode carbon corrosion and PEM degradation [295,299].

Robin et al. [358] presented an indirect coupling approach of a performance model and catalyst degradation. A local platinum dissolution model was used to calculate the degradation rates for various local conditions. These values for the degradation rate were then stored in a four-dimensional look-up table. Afterwards this look-up table was used in a higher scale model that is able to simulate the local conditions depending on the operating conditions. Given these simulated local conditions, the degradation rate is provided by the look-up table. The advantage of such an indirect coupling is that the simulation time can be reduced significantly since the degradation look-up table only has to be created once. However, especially for complex degradation mechanisms, the dimension of such a look-up table might become very large, due to the large number of parameters entering the degradation rates. Thus, the indirect coupling methodology is feasible especially for simplified degradation models.

## 4. Summary and perspectives

PEMFC are a promising alternative to conventional energy conversion systems. However, there is still a need of improvement in durability and cost reduction. The development of validated PEMFC models is crucial for solving these issues, by providing profound insights into the relevant processes. In general, a main challenge for modeling these processes is the wide range of scales which has to be covered, ranging from the atomistic level up to the system level. Depending on the scale very different model approaches have to be applied. Furthermore, a consistent way of coupling these models has to be established in order to derive a predictive multiscale PEMFC model.

During the last two decades, significant efforts in various European laboratories have been devoted to the theoretical description of idealistic elementary mechanism of oxygen reduction reaction on the basis of density functional theory calculations at the atomic scale. Although the catalyst and active site models are usually simplified (extended metallic surfaces in contact with a gas), this approach has helped to advance in the knowledge of the catalyst performance. Up to date, an explicit theoretical description of the catalytic environment at the atomic scale is missing (solvent, support, electric field, interface with the polymer membrane etc. . .). In addition, the study of the complex morphology of the metallic nanoparticles and its influence on the catalytic properties are open questions. For the ab initio approaches, the challenges at short term are thus related to the extension of the state-of-the-art models (gas/metal models) to the complex interfaces between the catalyst nanoparticles, the solvent environment, the graphitic support and the polymer membrane. The difficulty is not only the elaboration of those interfaces (large chemical systems involving thousands of atoms and ten thousands of electrons) and the required calculation time but also the development of an adapted methodology for treating correctly the electronic interactions at stake, especially dispersion and more generally polarization. Another promising way to improve the atomistic models and to check their validity is the implementation of kinetic rate constants in mesoscale stochastic simulations able to explore the catalytic activity at a larger scale by combining all the elementary acts of the reaction mechanism. Preliminary efforts have been conceded in this way and the challenges at midterm are thus the coupling between those approaches. At long term, the ab initio methodology will have to be extended to describe properly thermodynamics and kinetics of ORR with the presence of an external electric field. Current phenomenological models have been proposed in the literature to take into account such an environment effect without clearly solving the ongoing questions. The feedback of mesoscale simulations at this level will certainly be crucial to progress on this difficult task.

The high computational demand of micro- and mesoscale simulations necessitates the introduction of different modeling approaches when considering the whole cell. Such cell models, which consider the transport on the macro scale, are needed to optimize durability and performance of PEMFC. Different cell models have been proposed in recent years, usually focusing on a certain topic like the effect of liquid water (flooding) or the effect of the flow-field design. Depending on this focus other effects often have been neglected in order to simplify the model. Furthermore, empirical relations are necessary in these models, since the coupling to lower scale models is usually missing. These simplifications and empirical relations, however, limit the predictability of these models.

More detailed macroscale models have been developed for certain cell components. The models presented for the membrane transport mainly differ from each other by the transport mechanisms proposed for water and protons. For water concentration gradients, pressure gradients or more general gradients in chemical potential are considered as driving force. In addition the electro-osmotic drag is taken into account. For protons different transport mechanisms have been discussed (e.g. en masse diffusion, surface diffusion and Grotthuss mechanism). Concerning the water sorption of the membrane, different models have been proposed to describe the so-called Schroeder's paradox, i.e., the apparent difference of water sorption in contact with liquid water compared to saturated vapor. However, the true nature of this phenomenon and even its existence are still under debate.

Depending on the required accuracy, macroscale models of very different complexity have been developed for the catalyst layer. The easiest possibility is to consider the electrode as a thin interface between the membrane and the GDL, neglecting all transport phenomena within the catalyst layer. Macrohomogeneous models consider transport within the CL according to Darcy's law. However, assuming a homogeneous mixture of all phases neglects effects of the agglomerate structure of the electrode. These effects are taken into account by agglomerate models, where the agglomerates are considered to be spherical or cylindrical. It turns out that these models are able to accurately describe all domains of the polarization curve. Especially at high current density, transport limitations within the agglomerates become relevant. Using Pore Network Models or Direct Numerical Simulations allows studying the effect of the real electrode structure in detail, but requires much higher computational effort.

For the gas diffusion layer, different modeling approaches are considered to describe the two phase transport. The Continuum Models are again based on Darcy's law. However, since the pore size is not significantly smaller than the width of the GDL, this porous media approach might be not very accurate. On the other hand Direct Numerical Simulations of the GDL are computationally demanding. Powerful alternatives are provided by Pore Network models and the Lattice Boltzmann method. Both of them can also be used to derive effective transport parameters for macro models, i.e., contribute to the development of multiscale models.

The interface between the porous GDL and the gas flow channel has been subject of many investigations due to its importance for the water managements. Here, models focus in particular on the droplet formation and droplet detachment which occurs on this boundary. These models allow investigating the effect of GDL and channel properties as well as of operating conditions on the droplet behavior. Due to the complexity of these models, they typically only include the GDL and channel domains but not the whole cell.

Turning to higher scales, i.e., to the stack and system level, models are required which can be integrated into a controller for optimization of performance and durability under given operating conditions. These models have to be simplified in order to keep the computation time within the control period. The challenge is to achieve this without losing the effect of relevant mechanisms. Multiscale models are necessary to reach this goal.

In principle two different approaches are possible to develop multiscale models. One possibility is the direct coupling of two models on different scales, e.g., a continuum model describing the transport on the macro scale can be coupled with kinetic Monte Carlo model describing the electrochemical reactions. However, such a direct coupling is computationally demanding. Alternatively, lower scale models can be used for the parameterization of the higher scale models. Such an indirect coupling significantly reduces the computational costs, since once the parameters have been determined, only effective macroscale simulations have to be performed.

Predictive modeling of PEMFC degradation mechanisms is of major importance for further improvements of this technology, but also poses a particular challenge. Not only the degradation mechanisms themselves have to be modeled accurately, they also have to be coupled to a detailed cell model in order obtain the correct local conditions driving the degradation. Furthermore, the degradation

mechanisms often cannot be considered to be independent but interacting.

For the membrane, in principle three different degradation mechanisms can be considered: Thermal degradation, mechanical degradation and chemical degradation. Thermal degradation is believed to be negligible under standard operating conditions and has not been addressed so far in modeling works. Mechanical degradation can be caused by stresses resulting from repeated swelling and shrinking of the membrane due to water sorption and desorption. Consequently, models have been developed which are able to describe the mechanical membrane properties depending on parameters like temperature, humidity and strain rate. These models allow investigating the stresses within the membrane. However, predictive models describing, e.g., the formation of cracks and pinholes, are still to be developed. The chemical degradation of the membrane, i.e., the decomposition due to (electro-) chemical reactions, is believed to be the most severe degradation mechanism for the membrane. Consequently, several 0D and 1D models describing the chemical degradation have been developed. However, little has been done so far in the challenging task to couple this degradation to the transport properties of the membrane. Furthermore, advanced models taking into account the coupling between mechanical and chemical degradation have to be developed.

An important issue for the catalyst layer is the loss of electrochemical active surface area during operation. Several models have been developed to describe the responsible mechanisms. One approach accounts the loss of ECSA to the dissolution of the platinum particles. However, experimentally a growth of the average particle size and consequent stabilization of the catalyst is observed. This can be explained by the so called Ostwald-ripening mechanism, where dissolved $Pt^{2+}$ ions precipitate on the larger particles leading to an effective growth of the average particles and a reduction of the surface. While there is agreement about the importance of platinum oxide formation/reduction on the platinum dissolution kinetics, recent experiments suggest that the models describing the effect of the oxides might be oversimplified. Both, the oxide models themselves and their coupling with the platinum dissolution, have to be improved in order to be able to predict the catalyst degradation under transient conditions. Furthermore, the relevance of the coalescence mechanism for the particle growth is still under debate. While dissolution and Ostwald-ripening are usually considered in the literature, coalescence is typically not included in the models so far. Another mechanism which plays an important role in the degradation of the CL is carbon corrosion. On the one hand, it can cause a detachment of platinum particles, leading to a reduction of the ECSA. On the other hand, it can reduce the oxygen transport and promote flooding due to structural changes in the CL. Several models have been developed to study the effect of start-up and shutdown and fuel starvation on the carbon corrosion rates. Similar to the membrane degradation models, most of the proposed degradation models for the CL are decoupled from the performance of the cell, therefore cannot be used for lifetime prediction. Only recently, some models have been developed which explicitly take into account the coupling between performance and degradation as well as the coupling between several aging mechanisms.

In the GDL the loss of hydrophobicity due to PTFE degradation is of particular importance, since it promotes the flooding of the cathode. Some models have been presented which discuss the effect of the hydrophobicity loss on the liquid water transport and on the cell performance, while the mechanisms behind the hydrophobicity loss during aging has not yet been modeled so far.

Degradation of the bipolar plate by means of oxide layer formation or corrosion of the constituent materials leads to a loss of stack performance due to an increase of the interfacial contact resistance between GDL and BPP. Only a few models for this contact resistance have been developed so far, however, none of them includes degradation.

Summarizing, it can be said that a lot of work has been done so far in the modeling of PEMFC components performance and degradation on all relevant scales. The complexity of the available models on all scales increases consistently by taking into account more and more relevant mechanisms. In addition progress is made in coupling on the one hand the models at different scales and on the other hand the performance and degradation models. In order to pave the way to real predictive PEMFC models, still a lot of work has to be done in identifying and quantifying the relevance of certain mechanisms, e.g., for platinum oxides or the coalescence mechanism. Furthermore, mechanisms which have been considered only separately until now, have to be combined within multiscale models to capture the complex interplay between all relevant processes. Anyhow, models have in various cases already shown great capability in providing very good predictions in how fuel cell designs will perform in real life. This can reduce the number of designs that need to be built and tested. In the end, an effectively used and calibrated model leads to cost savings from cutting down on experimental trial and error time, materials, and manpower. Furthermore, the development of controllers based on multiscale models is expected to yield improved performance and durability of PEMFC.

However, despite advances in modeling, there is evidence that during the race to market with commercially viable designs, industrial organizations still tend to favor empirical experimentation over meticulous modeling and simulation. The key reason for this might be the lack of understanding or access to modern modeling frameworks being proposed by scientists in universities or research institutions. Depending on the size of a company and access to recent PhD graduates, a lack of access to up to date modeling expertise and expense of gaining access to peer reviewed academic content is a barrier to some industrial establishments using modeling. This slowly changes with the researcher mobility between academia and industry, who respectively bring their simulation and application knowledge with them. One way that the academic and industrial worlds interface is co-funded collaborative research programs. This is usually a win–win partnership as the industrial partner benefits from subsidized access to the latest understanding and modeling tools, while the researchers and students gain experience applying them in real applications.

## Acknowledgments

The research leading to this review has been partially supported by the European Union's Seventh Framework Program for the Fuel Cells and Hydrogen Joint Technology Initiative under the project PUMA MIND (grant agreement no 303419). Responsibility for the information and views set out in this review lies entirely with the authors.

## References

[1] A.Z. Weber, R.L. Borup, R.M. Darling, P.K. Das, T.J. Dursch, W. Gu, D. Harvey, A. Kusoglu, S. Litster, M.M. Mench, R. Mukundan, J.P. Owejan, J.G. Pharoah, M. Secanell, I.V. Zenyuk, J. Electrochem. Soc. 161 (2014), F1254.
[2] M. Bavarian, M. Soroush, I.G. Kevrekidis, J.B. Benziger, Ind. Eng. Chem. Res. 49 (2010) 7922.
[3] A. Biyikoglu, Int. J. Hydrogen Energy 30 (2005) 1181.
[4] D. Cheddie, N. Munroe, J. Power Sources 147 (2005) 72.
[5] A.Z. Weber, J. Newman, Chem. Rev. 104 (2004) 4679.
[6] H. Li, Y. Tang, Z. Wang, Z. Shi, S. Wu, D. Song, J. Zhang, K. Fatih, H. Wang, Z. Liu, R. Abouatallah, A. Mazza, J. Power Sources 178 (2008) 103.
[7] S. Mazumder, J.V. Cole, J. Electrochem. Soc. 150 (2003) A1510.
[8] L. Carrette, K.A. Friedrich, U. Stimming, ChemPhysChem 1 (2000) 162.
[9] J. Greeley, I.E.L. Stephens, A.S. Bondarenko, T.P. Johansson, H.A. Hansen, T.F. Jaramillo, J. Rossmeisl, I. Chorkendorff, J.K. Nørskov, Nat. Chem. 1 (2009) 552.
[10] N.M. Markovic, P.N. Ross Jr., Surf. Sci. Rep. 45 (2002) 117.

[11] V.R. Stamenkovic, B. Fowler, B.S. Mun, G. Wang, P.N. Ross, C.A. Lucas, N.M. Markovic, Science 315 (2007) 493.
[12] H.A. Gasteiger, S.S. Kocha, B. Sompalli, F.T. Wagner, Appl. Catal. B Environ. 56 (2005) 9.
[13] C.V. Rao, B. Viswanathan, J. Phys. Chem. C 114 (2010) 8661.
[14] S.W. Lee, S. Chen, J. Suntivich, K. Sasaki, R.R. Adzic, Y. Shao-Horn, J. Phys. Chem. Lett. 1 (2010) 1316.
[15] J.K. Nørskov, J. Rossmeisl, A. Logadottir, L. Lindqvist, J.R. Kitchin, T. Bligaard, H. Jónsson, J. Phys. Chem. B 108 (2004) 17886.
[16] F.J. Pérez-Alonso, D.N. McCarthy, A. Nierhoff, P. Hernández-Fernández, C. Strebel, I.E.L. Stephens, J.H. Nielsen, I. Chorkendorff, Angew. Chem. Int. Ed. 51 (2012) 4641.
[17] I.E.L. Stephens, A.S. Bondarenko, U. Gronbjerg, J. Rossmeisl, I. Chorkendorff, Energy Environ. Sci. 5 (2012) 6744.
[18] K. Yamamoto, T. Imaoka, W.-J. Chun, O. Enoki, H. Katoh, M. Takenaga, A. Sonoi, Nat. Chem. 1 (2009) 397.
[19] A.I. Yanson, P. Rodríguez, N. García-Aráez, R.V. Mom, F.D. Tichelaar, M.T.M. Koper, Angew. Chem. Int. Ed. 50 (2011) 6346.
[20] O. Antoine, Y. Bultel, R. Durand, P. Ozil, Electrochim. Acta 43 (1998) 3681.
[21] K.F. Blurton, P. Greenberg, H.G. Oswin, D.R. Putt, J. Electrochem. Soc. 119 (1972) 559.
[22] H.I. Zeliger, J. Electrochem. Soc. 114 (1967) 144.
[23] A.S. Bandarenka, H.A. Hansen, J. Rossmeisl, E.L. Stephens, Phys. Chem. Chem. Phys. 16 (2014) 13625–13629.
[24] F. Calle-Vallejo, M.T.M. Koper, Electrochim. Acta 84 (2012) 3.
[25] H.A. Hansen, J. Rossmeisl, J.K. Norskov, Phys. Chem. Chem. Phys. 10 (2008) 3722.
[26] V. Tripkovic, E. Skúlasona, S. Siahrostamia, J.K. Nørskov, J. Rossmeisl, Electrochim. Acta 55 (2010) 7975.
[27] M.T.M. Koper, Chem. Sci. 4 (2013) 2710.
[28] M.T.M. Koper, Phys. Chem. Chem. Phys. 15 (2012) 1399.
[29] J. Rossmeisl, K. Chan, R. Ahmed, V. Tripkovic, M.E. Bjorketun, Phys. Chem. Chem. Phys. 15 (2013) 10321.
[30] S. Walch, A. Dhanda, M. Aryanpour, H. Pitsch, J. Phys. Chem. C 112 (2008) 8464.
[31] A. Roudgar, M. Eikerling, R. van Santen, Phys. Chem. Chem. Phys. 12 (2010) 614.
[32] L. Wang, A. Roudgar, M. Eikerling, J. Phys. Chem. C 113 (2009) 17989.
[33] B.C. Han, C.R. Miranda, G. Ceder, Phys. Rev. B 77 (2008) 9.
[34] F. Calle-Vallejo, J.I. Martínez, J.M. García-Lastra, P. Sautet, D. Loffreda, Angew. Chem. Int. Ed. 53 (2014) 8316.
[35] F. Calle-Vallejo, P. Sautet, D. Loffreda, J. Phys. Chem. Lett. 5 (2014) 3120.
[36] F. Calle-Vallejo, J. Tymoczko, V. Colic, Q. Huy Vu, M.D. Pohl, K. Morgenstern, D. Loffreda, P. Sautet, W. Schuhmann, A.S. Bandarenka, Science 350 (2015) 185.
[37] Y. Sha, T.H. Yu, Y. Liu, B.V. Merinov, W.A. Goddard, J. Phys. Chem. Lett. 1 (2010) 856.
[38] A. Michaelides, P. Hu, J. Am. Chem. Soc. 123 (2001) 4235.
[39] R. Ferreira de Morais, A.A. Franco, P. Sautet, D. Loffreda, ACS Catal. 5 (2015) 1068.
[40] R. Ferreira de Morais, A.A. Franco, P. Sautet, D. Loffreda, Phys. Chem. Chem. Phys. 17 (2015) 11392.
[41] G.A. Tritsaris, J. Greeley, J. Rossmeisl, J.K. Norskov, Catal. Lett. 141 (2011) 909.
[42] V. Tripkovic, I. Cerri, T. Bligaard, J. Rossmeisl, Catal. Lett. 144 (2014) 380.
[43] J. Rossmeisl, E. Skulason, M.E. Björketun, V. Tripkovic, J.K. Norskov, Chem. Phys. Lett. 466 (2008) 68.
[44] S. Völkening, K. Bedürftig, K. Jacobi, J. Wintterlin, G. Ertl, Phys. Rev. Lett. 83 (1999) 2672.
[45] K. Bedürftig, S. Völkening, Y. Wang, J. Wintterlin, K. Jacobi, G. Ertl, J. Chem. Phys. 111 (1999) 11147.
[46] L.K. Verheij, M.B. Hugenschmidt, Surf. Sci. 416 (1998) 37.
[47] J. Biener, E. Lang, C. Lutterloh, J. Küppers, J. Chem. Phys. 116 (2002) 3063.
[48] D.C. Ford, A.U. Nilekar, Y. Xu, M. Mavrikakis, Surf. Sci. 604 (2010) 1565.
[49] I.E.L. Stephens, A.S. Bondarenko, F.J. Perez-Alonso, F. Calle-Vallejo, L. Bech, T.P. Johansson, A.K. Jepsen, R. Frydendal, B.P. Knudsen, J. Rossmeisl, I. Chorkendorff, J. Am. Chem. Soc. 133 (2011) 5485.
[50] R. Jinnouchi, K. Kodama, T. Hatanaka, Y. Morimoto, Phys. Chem. Chem. Phys. 13 (2011) 21070.
[51] R.F. de Morais, P. Sautet, D. Loffreda, A.A. Franco, Electrochim. Acta 56 (2011) 10842.
[52] A. Eichler, J. Hafner, Phys. Rev. Lett. 79 (1997) 4481.
[53] A. Eichler, F. Mittendorfer, J. Hafner, Phys. Rev. B 62 (2000) 4744.
[54] P. Gambardella, Z. Sljivancanin, B. Hammer, M. Blanc, K. Kuhnke, K. Kern, Phys. Rev. Lett. 87 (2001) 4.
[55] Y. Xu, A.V. Ruban, M. Mavrikakis, J. Am. Chem. Soc. 126 (2004) 4717.
[56] A. Michaelides, P. Hu, J. Am. Chem. Soc. 122 (2000) 9866.
[57] A. Michaelides, P. Hu, J. Chem. Phys. 114 (2001) 513.
[58] L. Qi, J. Yu, J. Lia, J. Chem. Phys. 125 (2006) 8.
[59] S. Kandoi, A.A. Gokhale, L.C. Grabow, J.A. Dumesic, M. Mavrikakis, Catal. Lett. 93 (2004) 93.
[60] Y. Wang, P.B. Balbuena, J. Phys. Chem. B 108 (2004) 4376.
[61] T. Jacob, W.A. Goddard, J. Am. Chem. Soc. 126 (2004) 9360.
[62] Y. Wang, P.B. Balbuena, J. Phys. Chem. B 109 (2005) 14896.
[63] Z. Gu, P.B. Balbuena, J. Phys. Chem. C 111 (2007) 17388.
[64] M. Otani, I. Hamada, O. Sugino, Y. Morikawa, Y. Okamotode, T. Ikeshoji, Phys. Chem. Chem. Phys. 10 (2008) 3609.
[65] L. Ou, F. Yang, Y. Liu, S. Chen, J. Phys. Chem. C 113 (2009) 20657.
[66] J.M.M. de la Hoz, D.F. Leon-Quintero, P. Hirunsit, P.B. Balbuena, Chem. Phys. Lett. 498 (2010) 328.
[67] R. Callejas-Tovar, W. Liao, J.M.M. de la Hoz, P.B. Balbuena, J. Phys. Chem. C 115 (2011) 4104.
[68] J.-S. Filhol, M. Neurock, Angew. Chem. Int. Ed. 45 (2006) 402.
[69] G.S. Karlberg, J. Rossmeisl, J.K. Nørskov, Phys. Chem. Chem. Phys. 9 (2007) 5158.
[70] A.U. Nilekar, M. Mavrikakis, Surf. Sci. 602 (2008) L89.
[71] M.J. Janik, C.D. Taylor, M. Neurock, J. Electrochem. Soc. 156 (2009) B126.
[72] J.A. Keith, G. Jerkiewicz, T. Jacob, ChemPhysChem 11 (2010) 2779.
[73] E. Skulason, V. Tripkovic, M.E. Björketun, S. Gudmundsdottir, G. Karlberg, J. Rossmeisl, T. Bligaard, H. Jonsson, J.K. Nørskov, J. Phys. Chem. C 114 (2010) 18182.
[74] A.S. Bondarenko, I.E.L. Stephens, H.A. Hansen, F.J. Perez-Alonso, V. Tripkovic, T.P. Johansson, J. Rossmeisl, J.K. Nørskov, I. Chorkendorff, Langmuir 27 (2011) 2058.
[75] K.-Y. Yeh, M.J. Janik, J. Comput. Chem. 32 (2011) 3399.
[76] A.A. Franco, S. Passot, P. Fugier, E. Billy, N. Guillet, L. Guetaz, E. De Vito, S. Mailley, J. Electrochem. Soc. 156 (2009) B410.
[77] A.A. Franco, P. Schott, C. Jallut, B. Maschke, Fuel Cells 7 (2007) 99.
[78] I.C. Man, H.Y. Su, F. Calle-Vallejo, H.A. Hansen, J.I. Mart'nez, N.G. Inoglu, J. Kitchin, T.F. Jaramillo, J.K. Norskov, J. Rossmeisl, ChemCatChem 3 (2011) 1159.
[79] F. Calle-Vallejo, D. Loffreda, M.T.M. Koper, P. Sautet, Nat. Chem. 7 (2015) 403.
[80] A.A. Franco, In: C. Hartnig, C. Roth (Eds.), Polym. Electrolyte Membr. Direct Methanol Fuel Cell Technol., Woodhead, UK, 2012.
[81] J.K. Norskov, T. Bligaard, J. Rossmeisl, C.H. Christensen, Nat. Chem. 1 (2009) 37.
[82] A.N. Frumkin, Acta Physicochim. URSS 18 (1943) 23.
[83] A.A. Franco, P. Schott, C. Jallut, B. Maschke, J. Electrochem. Soc. 153 (2006) A1053.
[84] A.A. Franco, In: I. Kondov, G. Sutmann (Eds.), Multiscale Model. Methods Appl. Mater. Sci., CECAM & FZ Jülich, Germany, 2013.
[85] A.A. Franco, In: R. Savinell, K.I. Ota, G. Kreysa (Eds.), Encycl. Appl. Electrochem., Springer, UK, 2013.
[86] R. He, S. Chen, F. Yang, B. Wu, J. Phys. Chem. B 110 (2006) 3262.
[87] C.O. Laoire, S. Mukerjee, K.M. Abraham, E.J. Plichta, M.A. Hendrickson, J. Phys. Chem. C 114 (2010) 9178.
[88] M.A. Quiroga, K.-H. Xue, T.-K. Nguyen, M. Tulodziecki, H. Huang, A.A. Franco, J. Electrochem. Soc. 161 (2014) E3302.
[89] K. Reuter, In: O. Deutschmann (Ed.), Model. Simul. Heterog. Catal. React. From Mol. Process to Tech. Syst., Wiley-VCH, Weinberg, 2011.
[90] N.G. Van Kampen, Stochastic Processes in Physics and Chemistry, 1992, Access Online via Elsevier.
[91] D.T. Gillespie, J. Comput. Phys. 22 (1976) 403.
[92] A.P.J. Jansen, Comput. Phys. Commun. 86 (1995) 1.
[93] R. Rico-Martínez, C.W. Gear, I.G. Kevrekidis, J. Comput. Phys. 196 (2004) 474.
[94] H.S. Casalongue, S. Kaya, V. Viswanathan, D.J. Miller, D. Friebel, H.A. Hansen, J.K. Nørskov, A. Nilsson, H. Ogasawara, Nat. Commun. 4 (2013).
[95] J. Lukkien, J. Segers, P. Hilbers, R. Gelten, a. Jansen, Phys. Rev. E 58 (1998) 2598.
[96] V.P. Zhdanov, J. Electroanal. Chem. 607 (2007) 17.
[97] L.A. Abramova, A.V. Zeigarnik, S.P. Baranov, E. Shustorovich, Surf. Sci. 565 (2004) 45.
[98] V. Rai, M. Aryanpour, H. Pitsch, J. Phys. Chem. C 112 (2008) 9760.
[99] J.X. Wang, N.M. Markovic, R.R. Adzic, J. Phys. Chem. B 108 (2004) 4127.
[100] M.A. Quiroga, A.A. Franco, J. Electrochem. Soc. 162 (2015) E73.
[101] W. Goddard III, B. Merinov, A. Van Duin, T. Jacob, M. Blanco, V. Molinero, S.S. Jang, Y.H. Jang, Mol. Simul. 32 (2006) 251.
[102] M. Uchida, Y. Aoyama, N. Eda, A. Ohta, J. Electrochem. Soc. 142 (1995) 463.
[103] M. Uchida, Y. Aoyama, N. Eda, A. Ohta, J. Electrochem. Soc. 142 (1995) 4143.
[104] M. Uchida, Y. Fukuoka, Y. Sugawara, N. Eda, A. Ohta, J. Electrochem. Soc. 143 (1996) 2245.
[105] D. Marx, M.E. Tuckerman, J. Hutter, M. Parrinello, Nature 397 (1999) 601.
[106] M. Tuckerman, K. Laasonen, M. Sprik, M. Parrinello, J. Phys. Chem. 99 (1995) 5749.
[107] M. Eikerling, A.A. Kornyshev, A.A. Kulikovsky, Electrochem. Eng. 5 (2007) 447.
[108] M. Eikerling, A.S. Ioselevich, A.A. Kornyshev, Fuel Cells 4 (2004) 131.
[109] K. Malek, M. Eikerling, Q. Wang, T. Navessin, Z. Liu, J. Phys. Chem. C 111 (2007) 13627.
[110] J.T. Wescott, Y. Qi, L. Subramanian, T.W. Capehart, J. Chem. Phys. 124 (2006) 134702.
[111] D. Damasceno Borges, K. Malek, S. Mossa, G. Gebel, A.A. Franco, ECS Trans. 45 (2013) 101.
[112] A.A. Franco, A Physical Multiscale Model of the Electrochemical Dynamics in a Polymer Electrolyte Fuel Cell – an Infinite Dimensional Bond Graph Approach PhD thesis, Université Claude Bernard Lyon-1, France, 2005.
[113] K.-H. Xue, T.-K. Nguyen, A.A. Franco, J. Electrochem. Soc. 161 (2014) E3028.
[114] K. Malek, T. Mashio, M. Eikerling, Electrocatalysis 2 (2011) 141.
[115] T.E. Springer, T.A. Zawodzinski, S. Gottesfeld, J. Electrochem. Soc. 138 (1991) 2334.
[116] G. Maggio, V. Recupero, L. Pino, J. Power Sources 101 (2001) 257.
[117] P. Costamagna, Chem. Eng. Sci. 56 (2001) 323.
[118] S. Um, C.Y. Wang, Proc. ASME Fuel Cell Div. 7 (2000).
[119] S. Um, C.Y. Wang, J. Power Sources 125 (2004) 40.
[120] Y. Wang, C.Y. Wang, Electrochim. Acta 50 (2005) 1307.
[121] Y. Wang, C.Y. Wang, Electrochim. Acta 51 (2006) 3924.
[122] R. O'Hayre, S.-W. Cha, W. Colella, F.B. Prinz, Fuel Cell Fundamentals, second ed., John Wiley & Sons, New York, 2009.

[123] C. Vallieres, D. Winkelmann, D. Roizard, E. Favre, P. Scharfer, M. Kind, J. Memb. Sci. 278 (2006) 357.
[124] P.V. Schroeder, Z. Phys. Chem. 45 (1903) 75.
[125] L.M. Onishi, J.M. Prausnitz, J. Newman, J. Phys. Chem. B 111 (2007) 10166.
[126] S. Jeck, P. Scharfer, M. Kind, J. Memb. Sci. 373 (2011) 74.
[127] K.-D. Kreuer, Solid State Ionics 252 (2013) 93.
[128] P.W. Majsztrik, M.B. Satterfield, A.B. Bocarsly, J.B. Benziger, J. Memb. Sci. 301 (2007) 93.
[129] V. Freger, J. Phys. Chem. B 113 (2009) 24.
[130] P. Choi, R. Datta, J. Electrochem. Soc. 150 (2003) E601.
[131] P. Choi, N.H. Jalani, R. Datta, J. Electrochem. Soc. 152 (2005) E123.
[132] M.H. Eikerling, P. Berg, Soft Matter 7 (2011) 5976.
[133] P. Choi, N.H. Jalani, R. Datta, J. Electrochem. Soc. 152 (2005) E84.
[134] S. Ge, X. Li, B. Yi, I.-M. Hsing, J. Electrochem. Soc. 152 (2005) A1149.
[135] M.B. Satterfield, J.B. Benziger, J. Phys. Chem. B 112 (2008) 3693.
[136] T. Romero, W. Mérida, J. Memb. Sci. 338 (2009) 135.
[137] D.T. Hallinan, M.G. De Angelis, M. Giacinti Baschetti, G.C. Sarti, Y.A. Elabd, Macromolecules 43 (2010) 4667.
[138] T.J. Silverman, J.P. Meyers, J.J. Beaman, J. Electrochem. Soc. 157 (2010) B1376.
[139] T.J. Silverman, J.P. Meyers, J.J. Beaman, Fuel Cells 11 (2011) 875.
[140] B. Kientiz, H. Yamada, N. Nonoyama, A.Z. Weber, J. Fuel Cell Sci. Technol. 8 (2011) 011013.
[141] Q. He, A. Kusoglu, I.T. Lucas, K. Clark, A.Z. Weber, R. Kostecki, J. Phys. Chem. B 115 (2011) 11650.
[142] D.A. Caulk, A.M. Brenner, S.M. Clapham, J. Electrochem. Soc. 159 (2012) F518.
[143] D.M. Bernardi, M.W. Verbrugge, AIChE J. 37 (1991) 1151.
[144] D.M. Bernardi, M.W. Verbrugge, J. Electrochem. Soc. 139 (1992) 2477.
[145] R. Schlögl, U. Schödel, Z. Phys. Chem. 5 (1955) 372.
[146] M. Eikerling, J. Electrochem. Soc. 145 (1998) 2684.
[147] T.F. Fuller, J. Newman, J. Electrochem. Soc. 140 (1993) 1218.
[148] G.J.M. Janssen, J. Electrochem. Soc. 148 (2001) A1313.
[149] A.Z. Weber, J. Newman, J. Electrochem. Soc. 150 (2003) A1008.
[150] A.Z. Weber, J. Newman, J. Electrochem. Soc. 151 (2004) A326.
[151] T. Thampan, S. Malhotra, H. Tang, R. Datta, J. Electrochem. Soc. 147 (2000) 3242.
[152] E.A. Mason, A.P. Malinauskas, Gas Transp. Porous Media. Dusty-Gas Model, 1983, Amsterdam.
[153] J. Fimrite, H. Struchtrup, N. Djilali, J. Electrochem. Soc. 152 (2005) A1804.
[154] M.J. Moran, H.N. Shapiro, Fundamentals of Engineering Thermodynamics, John Wiley & Sons, New York, 1996.
[155] J. Fimrite, B. Carnes, H. Struchtrup, N. Djilali, J. Electrochem. Soc. 152 (2005) A1815.
[156] J.J. Baschuk, X. Li, Int. J. Hydrogen Energy 35 (2010) 5095.
[157] P.J. Flory, Principles of Polymer Chemistry, Cornell University Press, Ithaca, NY, 1953.
[158] Y.W. Rho, S. Srinivasan, Y.T. Kho, J. Electrochem. Soc. 141 (1994) 2089.
[159] M. Eikerling, J. Electrochem. Soc. 153 (2006) E58.
[160] P. Schott, P. Baurens, J. Power Sources 156 (2006) 85.
[161] S. Jomori, N. Nonoyama, T. Yoshida, J. Power Sources 215 (2012) 18.
[162] F.C. Cetinbas, S.G. Advani, A.K. Prasad, J. Electrochem. Soc. (2014) F803.
[163] Q. Yan, J. Wu, Energy Convers. Manag. 49 (2008) 2425.
[164] A.Z. Weber, J. Newman, J. Electrochem. Soc. 151 (2004) A311.
[165] D. Harvey, J.G. Pharoah, K. Karan, J. Power Sources 179 (2008) 209.
[166] S.M. Rao, Y. Xing, J. Power Sources 185 (2008) 1094.
[167] M.M. Hussain, D. Song, Z.-S. Liu, Z. Xie, J. Power Sources 196 (2011) 4533.
[168] F.C. Cetinbas, S.G. Advani, A.K. Prasadz, J. Electrochem. Soc. 160 (2013) F750.
[169] A. Suzuki, U. Sen, T. Hattori, R. Miura, R. Nagumo, H. Tsuboi, N. Hatakeyama, A. Endou, H. Takaba, M.C. Williams, A. Miyamoto, Int. J. Hydrogen Energy 36 (2011) 2221.
[170] G. Wang, P.P. Mukherjee, C.-Y. Wang, Electrochim. Acta 52 (2007) 6367.
[171] M. El Hannach, Simulation et Analyse Des Mécanismes de Transfert Diphasique Dans Les Couches Actives Des Piles À Combustible PEMFC, Institut National Polytechnique de Toulouse, 2011.
[172] S. Strahl, A. Husar, A.A. Franco, Int. J. Hydrogen Energy 39 (2014) 9752–9767.
[173] R.F. Mann, J.C. Amphlett, B.A. Peppley, C.P. Thurgood, J. Power Sources 161 (2006) 775.
[174] X. Cheng, Z. Shi, N. Glass, L. Zhang, J. Zhang, D. Song, Z.S. Liu, H. Wang, J. Shen, J. Power Sources 165 (2007) 739.
[175] D. Eberle, B. Horstmann, Electrochim. Acta 137 (2014) 714.
[176] A.A. Franco, Un Modele Physique Multiechelle de La Dynamique Electrochimique Dans Une Pile a Combustible a Electrolyte Polymore, Universite Claude Bernard – Lyon 1, 2005.
[177] S. Passot, Etude Expérimentale et Par Modélisation de L'impact D'impuretés de L'hydrogène Sur Le Fonctionnement Des Piles À Combustible À Membrane Échangeuse de Protons {(PEMFC)}, Université de Grenoble, 2012.
[178] J.X. Wang, J. Zhang, R.R. Adzic, J. Phys. Chem. A 111 (2007) 12702.
[179] A.Z. Weber, J. Newman, J. Electrochem. Soc. 152 (2005) A677.
[180] H. Meng, Int. J. Hydrogen Energy 34 (2009) 5488.
[181] P. Oberholzer, P. Boillat, R. Siegrist, A. Kästner, E.H. Lehmann, G.G. Scherer, A. Wokaun, Electrochem. Commun. 20 (2012) 67.
[182] A.Z. Weber, J. Newman, J. Electrochem. Soc. 153 (2006) A2205.
[183] N. Djilali, D. Lu, Int. J. Therm. Sci. 41 (2002) 29.
[184] A. Thomas, G. Maranzana, S. Didierjean, J. Dillet, O. Lottin, J. Electrochem. Soc. 160 (2013) F191.
[185] M. Andisheh-Tadbir, E. Kjeang, M. Bahrami, J. Power Sources 296 (2015) 344.
[186] J. Hermann, C. Ziegler, J. Electrochem. Soc. 155 (2010) B1066.
[187] M. Rebai, M. Prat, J. Power Sources 192 (2009) 534.
[188] J.H. Chun, K.T. Park, D.H. Jo, S.G. Kim, S.H. Kim, Int. J. Hydrogen Energy 36 (2011) 1837.
[189] N. Zamel, X. Li, Prog. Energy Combust. Sci. 39 (2013) 111.
[190] J. Pauchet, M. Prat, P. Schott, S.P. Kuttanikkad, Int. J. Hydrogen Energy 37 (2012) 1628.
[191] X. Zhang, Y. Gao, H. Ostadi, K. Jiang, R. Chen, Int. J. Hydrogen Energy 39 (2014) 17222.
[192] J. Ma, X. Zhang, Z. Jiang, H. Ostadi, K. Jiang, R. Chen, Fuel 136 (2014) 307.
[193] P.P. Mukherjee, Q. Kanga, C.Y. Wang, Energy Environ. Sci. 4 (2010) 346.
[194] X.D. Niu, T. Munekata, S.A. Hyodo, K. Suga, J. Power Sources 172 (2007) 542.
[195] Y. Tabe, Y. Lee, T. Chikahisa, M. Kozakai, J. Power Sources 193 (2009) 24.
[196] T. Koido, T. Furusawa, K. Moriyama, J. Power Sources 175 (2008) 127.
[197] B. Han, H. Meng, Int. J. Hydrogen Energy 38 (2013) 5053.
[198] K.N. Kim, J.H. Kang, S.G. Lee, J.H. Nam, C.-J. Kim, J. Power Sources 278 (2015) 703.
[199] G.R. Molaeimanesh, M.H. Akbari, Int. J. Hydrogen Energy 39 (2014) 8401.
[200] G.R. Molaeimanesh, M.H. Akbari, J. Power Sources 258 (2014) 89.
[201] P.A. García-Salaberri, J.T. Gostick, G. Hwang, A.Z. Weber, M. Vera, J. Power Sources 296 (2015) 440.
[202] K.S. Chen, M.A. Hickner, D.R. Noble, Int. J. Energy Res. 29 (2005) 1113.
[203] S.C. Cho, Y. Wang, K.S. Chen, J. Power Sources 206 (2012) 119.
[204] S.C. Cho, Y. Wang, K.S. Chen, J. Power Sources 210 (2012) 191.
[205] E.C. Kumbur, K.V. Sharp, M.M. Mench, J. Power Sources 161 (2006) 333.
[206] A. Theodorakakos, T. Ous, M. Gavaises, J.M. Nouri, J. Colloid Interface Sci. 300 (2006) 673.
[207] F.Y. Zhang, X.G. Yang, C.-Y. Wang, J. Electrochem. Soc. 153 (2006) A225.
[208] K.S. Chen, Proc. Fuel Cell (2008) 797.
[209] G. He, P. Ming, Z. Zhao, A. Abudula, Y. Xiao, J. Power Sources 163 (2007) 864.
[210] P. Polverino, A. Esposito, C. Pianese, Int. J. Hydrogen Energy 38 (2013) 8934.
[211] Z.H. Wang, C.Y. Wang, K.S. Chen, J. Power Sources 94 (2001) 40.
[212] M. Mortazavi, K. Tajiri, J. Power Sources 245 (2014) 236.
[213] E.C. Kumbur, K.V. Sharp, M.M. Mench, J. Electrochem. Soc. 154 (2007) B1315.
[214] A. Esposito, A. Montello, C. Pianese, Y.G. Guezennec, J. Fuel Cell Sci. Technol. 7 (2010) 031021.
[215] A. Esposito, C. Pianese, Y.G. Guezennec, J. Power Sources 195 (2010) 4149.
[216] A. Esposito, A.D. Montello, C. Pianese, Y.G. Guezennec, J. Power Sources 195 (2010) 2691.
[217] J.T. Pukrushpan, A.G. Stefanopoulou, H. Peng, Control of Fuel Cell Power Systems: Principles, Modeling, Analysis, and Feedback Design, Springer, 2004.
[218] Y. Shan, S.-Y. Choe, J. Power Sources 158 (2006) 274.
[219] C.H. Chen, S.P. Jung, S.C. Yen, J. Power Sources 173 (2007) 249.
[220] A. Miotti, A. Di Domenico, A. Esposito, Y.G. Guezennec, In: Proc. ASME 2006 Fourth Int. Conf. Fuel Cell Sci. Eng. Technol., 2006, p. 411.
[221] I. Arsie, A. Di Domenico, C. Pianese, M. Sorrentino, J. Fuel Cell Sci. Technol. 4 (2007) 261.
[222] I. Arsie, A. Di Domenico, C. Pianese, M. Sorrentino, J. Fuel Cell Sci. Technol. 7 (2010) 011004.
[223] R. Talj, D. Hissel, R. Ortega, M. Becherif, M. Hilairet, IEEE Trans. Ind. Electron 57 (2010) 1906.
[224] W.K. Na, B. Gou, Energy Convers. IEEE Trans. 23 (2008) 179.
[225] J. Zhang, G. Liu, W. Yu, M. Ouyang, J. Power Sources 179 (2008) 649.
[226] J. Hui, H. Jie, In: Int. Conf. Intell. Syst. Knowl. Eng., 2010, pp. 548–551.
[227] S. Strahl, N. Gasamans, J. Llorca, A. Husar, Int. J. Hydrogen Energy 39 (2014) 5378.
[228] C. Kunusch, A. Husar, P. Puleston, M. Mayosky, J. More, Int. J. Hydrogen Energy 33 (2008) 3581.
[229] C. Kunusch, P.F. Puleston, M.A. Mayosky, A.P. Husar, IEEE Trans. Energy Convers. 26 (2011) 851.
[230] M.Y. Ayad, M. Becherif, A. Henni, A. Aboubou, M. Wack, S. Laghrouche, Energy Convers. Manag. 51 (2010) 1468.
[231] D. Feroldi, M. Serra, J. Riera, J. Power Sources 190 (2009) 387.
[232] A.J. del Real, A. Arce, C. Bordons, In: 46th IEEE Conf. Decis. Control (CDC 2007), 2007, pp. 5447–5452.
[233] A.A. Franco, RSC Adv. 3 (2013) 13027.
[234] A.A. Franco, K.-H. Xue, ECS J. Solid State Sci. Technol. 2 (2013) M3084.
[235] C.Y. Wang, V. Srinivasan, J. Power Sources 110 (2002) 364.
[236] V. Viswanathan, F. Wang, H. Pitsch, Comput. Sci. Eng. 14 (2012) 60.
[237] K. Reuter, ChemInform 43 (2012).
[238] L. Madec, L. Falk, E. Plasari, Chem. Eng. Sci. 56 (2001) 1731.
[239] D. Sheppard, R. Terrell, G. Henkelman, J. Chem. Phys. 128 (2008) 134106.
[240] P. Maragakis, E. Kaxiras, In: APS Meet. Abstr., 2001, p. 15002.
[241] K. Malek, A.A. Franco, J. Phys. Chem. B 115 (2011) 8088.
[242] M.A. Quiroga, K. Malek, A.A. Franco, J. Electrochem. Soc. 163 (2015), F59.
[243] A.A. Franco, A Multiscale Modeling Framework for the Transient Analysis of Electrochemical Power Generators – from Theory to the Engineering Practice, Habilitation to Become Research Director (H.D.R.) Manuscript, Université Claude Bernard-Lyon I, France, 2010.
[244] A.A. Franco, Multiscale modeling of direct alcohol fuel cells, in: E. Gonzalez, H. Corti (Eds.), Direct Alcohol Fuel Cells Technologies: Research and Development, Springer, USA, 2013.
[245] http://www.modeling-electrochemistry.com/, 2013.
[246] W.G. Bessler, S. Gewies, M. Vogler, Electrochim. Acta 53 (2007) 1782.
[247] J.P. Neidhardt, D.N. Fronczek, T. Jahnke, T. Danner, B. Horstmann, W.G. Bessler, J. Electrochem. Soc. 159 (2012) A1528.
[248] M. Sarmiento, C. Batlle, I. Massana, M. Serra, In: Eur. Hydrog. Energy Conf., 2014, pp. 265–272.

[249] A. Collier, H. Wang, X. Ziyuan, J. Zhang, D. Wilkinson, Int. J. Hydrogen Energy 31 (2006) 1838.
[250] C.A. Wilkie, J.R. Thomsen, M.L. Mittleman, J. Appl. Polym. Sci. 42 (1991) 901.
[251] A. Alentiev, J. Kostina, G. Bondarenko, Desalination 200 (2006) 32.
[252] H.-L. Lin, T.L. Yu, C.-H. Huang, T.-L. Lin, J. Polym, Sci. Part B Polym. Phys. 43 (2005) 3044.
[253] H.F.M. Mohamed, Y. Kobayashi, C.S. Kuroda, A. Ohira, Macromol. Chem. Phys. 212 (2011) 708.
[254] R.C. McDonald, C.K. Mittelsteadt, E.L. Thompson, Fuel Cells 4 (2004) 208.
[255] R. Borup, J. Meyers, B. Pivovar, Y.S. Kim, R. Mukundan, N. Garland, D. Myers, M. Wilson, F. Garzon, D. Wood, P. Zelenay, K. More, K. Stroh, T. Zawodzinski, J. Boncella, J.E. McGrath, M. Inaba, K. Miyatake, M. Hori, K. Ota, Z. Ogumi, S. Miyata, A. Nishikata, Z. Siroma, Y. Uchimoto, K. Yasuda, K.-I. Kimijima, N. Iwashita, Chem. Rev. 107 (2007) 3904.
[256] A. Kusoglu, A.M. Karlsson, M.H. Santare, S. Cleghorn, W.B. Johnson, J. Power Sources 161 (2006) 987.
[257] Y. Tang, M.H. Santare, A.M. Karlsson, S. Cleghorn, W.B. Johnson, J. Fuel Cell Sci. Technol. 3 (2006) 119.
[258] M.F. Mathias, R. Makharia, H.A. Gasteiger, J.J. Conley, T.J. Fuller, C.J. Gittleman, S.S. Kocha, D.P. Miller, C.K. Mittelsteadt, T. Xie, S.G. Yan, P.T. Yu, Electrochem. Soc. Interface 14 (2005) 24.
[259] S.A. Vilekar, R. Datta, J. Power Sources 195 (2010) 2241.
[260] A.Z. Weber, J. Newman, AIChE J. 50 (2004) 3215.
[261] W. Yoon, X. Huang, J. Power Sources 196 (2011) 3933.
[262] A. Kusoglu, Y. Tang, M.H. Santare, A.M. Karlsson, S. Cleghorn, W.B. Johnson, J. Fuel Cell Sci. Technol. 6 (2009) 011012.
[263] Y.-H. Lai, C.K. Mittelsteadt, C.S. Gittleman, D. a. Dillard, J. Fuel Cell Sci. Technol. 6 (2009) 021002.
[264] M.N. Silberstein, M.C. Boyce, J. Power Sources 195 (2010) 5692.
[265] A. Kusoglu, Y. Tang, M. Lugo, A.M. Karlsson, M.H. Santare, S. Cleghorn, W.B. Johnson, J. Power Sources 195 (2010) 483.
[266] N.S. Khattra, Z. Lu, A.M. Karlsson, M.H. Santare, F.C. Busby, T. Schmiedel, J. Power Sources 228 (2013) 256.
[267] A. Kusoglu, M.H. Santare, A.M. Karlsson, S. Cleghorn, W.B. Johnson, J. Electrochem. Soc. 157 (2010) B705.
[268] V.V. Atrazhev, T.Y. Astakhova, D.V. Dmitriev, N.S. Erikhman, V.I. Sultanov, T. Patterson, S.F. Burlatsky, J. Electrochem. Soc. 160 (2013) F1129.
[269] M.N. Silberstein, M.C. Boyce, J. Power Sources 196 (2011) 3452.
[270] ABAQUS, 2003.
[271] T.T. Aindow, J. O'Neill, J. Power Sources 196 (2011) 3851.
[272] S.F. Burlatsky, M. Gummalla, J. O'Neill, V.V. Atrazhev, A.N. Varyukhin, D.V. Dmitriev, N.S. Erikhman, J. Power Sources 215 (2012) 135.
[273] G. Halsey, H.J. White, H. Eyring, Text. Res. J. 15 (1945) 295.
[274] K. Promislow, P. Chang, H. Haas, B. Wetton, J. Electrochem. Soc. 155 (2008) A494.
[275] A. Kusoglu, A.Z. Weber, J. Electrochem. Soc. 161 (2014) E3311.
[276] W. Liu, M. Crum, ECS Trans. 3 (2006) 531.
[277] M. Crum, W. Liu, ECS Trans. 3 (2006) 541.
[278] L. Ghassemzadeh, K.-D. Kreuer, J. Maier, K. Mu, J. Phys. Chem. C 114 (2010) 14635.
[279] T. Okada, In: W. Vielstich, H. Gasteiger, A. Lamm, H. Yokokawa (Eds), Handb. Fuel Cells – Fundam. Technol. Appl., John Wiley & Sons, Chichester, 2010.
[280] L. Gubler, S.M. Dockheer, W.H. Koppenol, J. Electrochem. Soc. 158 (2011) B755.
[281] C. Chen, T.F. Fuller, J. Electrochem. Soc. 156 (2009) B1218.
[282] M. Gummalla, V.V. Atrazhev, D. Condit, N. Cipollini, T. Madden, N.Y. Kuzminyh, D. Weiss, S.F. Burlatsky, J. Electrochem. Soc. 157 (2010) B1542.
[283] A.A. Shah, T.R. Ralph, F.C. Walsh, J. Electrochem. Soc. 156 (2009) B465.
[284] N. Ohguri, A.Y. Nosaka, Y. Nosaka, J. Power Sources 195 (2010) 4647.
[285] W. Liu, D. Zuckerbrod, J. Electrochem. Soc. 152 (2005) A1165.
[286] S. Kundu, M.W. Fowler, L.C. Simon, R. Abouatallah, N. Beydokhti, J. Power Sources 183 (2008) 619.
[287] L. Zhang, S. Mukerjee, J. Electrochem. Soc. 153 (2006) A1062.
[288] A. Ohma, S. Yamamoto, K. Shinohara, J. Power Sources 182 (2008) 39.
[289] M.P. Rodgers, L.J. Bonville, D.K. Slattery, ECS Trans. 41 (2011) 1461.
[290] N. Macauley, L. Ghassemzadeh, C. Lim, M. Watson, J. Kolodziej, M. Lauritzen, S. Holdcroft, E. Kjeang, ECS Electrochem. Lett. 2 (2013) F33.
[291] M.P. Rodgers, B.P. Pearman, L.J. Bonville, D.A. Cullen, N. Mohajeri, D.K. Slattery, J. Electrochem. Soc. 160 (2013) F1123.
[292] S. Helmly, B. Ohnmacht, R. Hiesgen, E. Gülzow, K.A. Friedrich, ECS Trans. 58 (2013) 969.
[293] S. Helmly, B. Ohnmacht, P. Gazdzicki, R. Hiesgen, E. Gülzow, K.A. Friedrich, J. Electrochem. Soc. 161 (2014) F1416.
[294] A.B. LaConti, A.R. Fragala, J.R. Boyack, In: S. Srinivasan, J.D.E. McIntyre, F.G. Will (Eds.), Proceeding Symp. Electrode Mater. Process Energy Convers. Storage, The Electrochemical Society, Princeton, 1977, pp. 354–374.
[295] V.A. Sethuraman, J.W. Weidner, A.T. Haug, S. Motupally, L.V. Protsailo, J. Electrochem. Soc. 155 (2008) B50.
[296] F. Haber, J. Weiss, Proc. R. Soc. Lond. A 134 (1934) 332.
[297] D.E. Curtin, R.D. Lousenberg, T.J. Henry, P.C. Tangeman, M.E. Tisack, J. Power Sources 131 (2004) 41.
[298] J. Healy, C. Hayden, T. Xie, K. Olson, R. Waldo, M. Brundage, H. Gasteiger, J. Abbott, Fuel Cells 5 (2005) 302.
[299] T. Xie, C.A. Hayden, Polymer (Guildf) 48 (2007) 5497.
[300] C. Chen, T.F. Fuller, Polym. Degrad. Stab. 94 (2009) 1436.
[301] T. Ishimoto, T. Ogura, M. Koyama, ECS Trans. 35 (2011) 1.
[302] J.M. Fenton, M.P. Rodgers, D.K. Slattery, X. Huang, V.O. Mittal, L.J. Bonville, H.R. Kunz, ECS Trans. 25 (2009) 233.
[303] T. Ishimoto, R. Nagumo, T. Ogura, T. Ishihara, B. Kim, A. Miyamoto, M. Koyama, J. Electrochem. Soc. 157 (2010) B1305.
[304] M. Ghelichi, P.-É.A. Melchy, M.H. Eikerling, J. Phys. Chem. B 118 (2014) 11375.
[305] http://www.psenterprise.com/, 2013.
[306] T. Madden, D. Weiss, N. Cipollini, D. Condit, M. Gummalla, S. Burlatsky, V. Atrazhev, J. Electrochem. Soc. 156 (2009) B657.
[307] R. Coulon, W.G. Bessler, A.A. Franco, ECS Trans. 25 (2010) 259.
[308] R. Coulon, Modeling of Chemical Degradation in Polymer Electrolyte Membrane Fuel Cells(PhD thesis), , Université de Grenoble, 2012.
[309] A.A. Franco, R. Coulon, R.F. de Morais, S.K. Cheah, A. Kachmar, M.A. Gabriel, ECS Trans. 25 (2009) 65.
[310] K.H. Wong, E. Kjeang, J. Electrochem. Soc. 161 (2014) F823.
[311] C. Lim, L. Ghassemzadeh, F. Van Hove, M. Lauritzen, J. Kolodziej, G.G. Wang, S. Holdcroft, E. Kjeang, J. Power Sources 257 (2014) 102–110.
[312] K.H. Wong, E. Kjeang, ChemSusChem 8 (2015) 1072.
[313] Y. Shao, G. Yin, Y. Gao, J. Power Sources 171 (2007) 558.
[314] A.P. Yadav, T. Okayasu, Y. Sugawara, A. Nishikata, T. Tsuru, J. Electrochem. Soc. 159 (2012) C190.
[315] R.M. Darling, J.P. Meyers, J. Electrochem. Soc. 150 (2003) A1523.
[316] R.M. Darling, J.P. Meyers, J. Electrochem. Soc. 152 (2005) A242.
[317] W. Bi, T.F. Fuller, J. Power Sources 178 (2008) 188.
[318] R.K. Ahluwalia, S. Arisetty, X. Wang, X. Wang, R. Subbaraman, S.C. Ball, S. DeCrane, D.J. Myers, J. Electrochem. Soc. 160 (2013) F447.
[319] A.A. Topalov, S. Cherevko, A.R. Zeradjanin, J.C. Meier, I. Katsounaros, K.J.J. Mayrhofer, Chem. Sci. 5 (2014) 631.
[320] S. Cherevko, A.R. Zeradjanin, G.P. Keeley, K.J.J. Mayrhofer, J. Electrochem. Soc. 161 (2014) H822.
[321] H. Angerstein-Kozlowska, B.E. Conway, W.B.A. Sharp, Electroanal. Chem. Interfacial Electrochem 43 (1973) 9.
[322] B.V. Tilak, B.E. Conway, H. Angerstein-Kozlowska, Electroanal. Chem. Interfacial Electrochem 48 (1973) 1.
[323] E.L. Redmond, B.P. Setzler, F.M. Alamgir, T.F. Fuller, Phys. Chem. Chem. Phys. 16 (2014) 5301.
[324] F. Behafarid, B. Roldan Cuenya, Top. Catal. 56 (2013) 1542.
[325] J.K. Seo, A. Khetan, M.H. Seo, H. Kim, B. Han, J. Power Sources 238 (2013) 137.
[326] P. Wynblatt, N.A. Gjostein, Acta Met. 24 (1976) 1165.
[327] M.C. Valero, P. Raybaud, P. Sautet, Phys. Rev. B 75 (2007) 045427.
[328] R. Ouyang, J.-X. Liu, W.-X. Li, J. Am. Chem. Soc. 135 (2013) 1760.
[329] A. Baldan, J. Mater. Sci. 37 (2002) 2171.
[330] P. Parthasarathy, A.V. Virkar, J. Power Sources 234 (2013) 82.
[331] T. Ous, C. Arcoumanis, J. Power Sources 240 (2013) 558.
[332] C.G. Granqvist, R.A. Buhrman, J. Catal. 42 (1976) 477.
[333] E. Ruckenstein, B. Pulvermacher, J. Catal. 29 (1973) 224.
[334] R.K. Ahluwalia, S. Arisetty, J.-K. Peng, R. Subbaraman, X. Wang, N. Kariuki, D.J. Myers, R. Mukundan, R. Borup, O. Polevaya, J. Electrochem. Soc. 161 (2014) F291.
[335] E.F. Holby, W. Sheng, Y. Shao-Horn, D. Morgan, Energy Environ. Sci. 2 (2009) 865.
[336] Y. Li, K. Moriyama, W. Gu, S. Arisetty, C.Y. Wang, J. Electrochem. Soc. 162 (2015) F834.
[337] P. Urchaga, T. Kadyk, S.G. Rinaldo, A.O. Pistono, J. Hu, W. Lee, C. Richards, M.H. Eikerling, C.A. Rice, Electrochim. Acta 176 (2015) 1500.
[338] A.A. Franco, M. Tembely, J. Electrochem. Soc. 154 (2007) B712.
[339] S. Knights, K. Colbow, J. St-Pierre, D. Wilkinson, J. Power Sources 127 (2004) 127.
[340] J.P. Meyers, R.M. Darling, J. Electrochem. Soc. 153 (2006) A1432.
[341] N. Takeuchi, T.F. Fuller, J. Electrochem. Soc. 155 (2008) B770.
[342] J. Hu, P.C. Sui, S. Kumar, N. Djilali, Electrochim. Acta 54 (2009) 5583.
[343] L. Guétaz, S. Escribano, O. Sicardy, J. Power Sources 212 (2012) 169.
[344] M. Schulze, N. Wagner, T. Kaz, K.A. Friedrich, Electrochem. Acta 52 (2007) 2328.
[345] J. Pauchet, M. Prat, P. Schott, S.P. Kuttanikkad, Int. J. Hydrogen Energy 37 (2012) 1628.
[346] K. Seidenberger, F. Wilhelm, T. Schmitt, W. Lehnert, J. Scholta, J. Power Sources 196 (2011) 5317.
[347] A. Casalegno, F. Bresciani, G. Groppi, R. Marchesi, J. Power Sources 196 (2011) 10632.
[348] D.A. Shores, G.A. Deluga, In: W. Vielstich, H.A. Gasteiger, A. Lamm (Eds.), Handb. Fuel Cells, Wiley, New York, 2003, pp. 273–285.
[349] J. Scherer, D. Münter, R. Ströbel, In: F.N. Büchi, M. Inaba, T.J. Schmidt (Eds.), Polym. Electrolyte Fuel Cell Durab., Springer, New York, 2009, pp. 243–255.
[350] R.A. Antunes, M.C.L. Oliveira, G. Ett, V. Ett, Int. J. Hydrogen Energy 35 (2010) 3632.
[351] P. Zhou, C.W. Wu, G.J. Ma, J. Power Sources 159 (2006) 1115.
[352] Z. Wu, Y. Zhou, G. Lin, S. Wang, S.J. Hu, J. Power Sources 182 (2008) 265.
[353] V. Mishra, F. Yang, R. Pitchumani, J. Fuel Cell Sci. Technol. 1 (2004) 2.
[354] L. Zhang, Y. Liu, H. Song, S. Wang, Y. Zhou, S.J. Hu, J. Power Sources 162 (2006) 1165.
[355] P. Marcus (Ed.), Corrosion Mechanisms in Theory and Practice, CRC Press, 2011.
[356] R.S. Munn (Ed.), Computer Modeling in Corrosion, ASTM International, 1992.
[357] J.P. Meyers, R.M. Darling, J. Electrochem. Soc. 153 (2006) A1432.
[358] C. Robin, M. Gerard, A.A. Franco, P. Schott, Int. J. Hydrogen Energy 38 (2013) 4675.
[359] N. Wagner, In: H. Wang, X.-Z. Yuan, H. Li (Eds.), PEM Fuel Cell Diagnostic Tools, CRC Press, Boca Raton, London, New York, 2012.

## List of abbreviations

*BoP:* Balance of Plant
*BPP:* Bipolar plate
*CCL:* Cathode Catalyst Layer
*CFD:* Computational Fluid Dynamics
*CG:* Coarse grained
*CGMD:* Coarse grained molecular dynamics
*CL:* Catalyst layer
*CM:* Continuum Models
*CNT:* Carbon nanotubes
*DFT:* Density Functional Theory
*ECSA:* Electrochemical surface area
*EDL:* Electrochemical double layer
*FC:* Fuel cell
*FER:* Fluoride emission rate
*GDL:* Gas diffusion layer
*GFC:* Gas flow channel
*HOR:* Hydrogen Oxidation Reaction
*kMC:* Kinetic Monte Carlo
*LBM:* Lattice Boltzmann method
*MEA:* Membrane Electrode Assembly
*MPL:* Micro Porous Layer
*NEB:* Nudged Elastic Band
*ORR:* Oxygen Reduction Reaction
*PBC:* Periodic boundary conditions
*PEMFC:* Polymer Electrolyte Membrane Fuel Cells
*PFSA:* Perfluorosulfonic acid
*PNM:* Pore Network Modeling
*PTFE:* Polytetrafluoroethylene
*RH:* Relative humidity
*RHE:* Reversible hydrogen electrode
*SEM:* Scanning electron microscopy